Physics of Fluids

RESEARCH ARTICLE | NOVEMBER 10 2023

# Motion of a solid particle in an ore-lifting riser with transverse vibrations

Mingzhu Wei (魏明珠) ; Jinlong Duan (段金龙) ; Xu Wang (王旭) ; Jifu Zhou (周济福)



*Physics of Fluids* 35, 113311 (2023)
https://doi.org/10.1063/5.0172324

Physics of Fluids ARTICLE pubs.aip.org/aip/pof

# Motion of a solid particle in an ore-lifting riser with transverse vibrations

Cite as: Phys. Fluids **35**, 113311 (2023); doi: 10.1063/5.0172324
Submitted: 14 August 2023 · Accepted: 19 October 2023 ·
Published Online: 10 November 2023

View Online Export Citation CrossMark

Mingzhu Wei (魏明珠),[1,2] Jinlong Duan (段金龙),[1] Xu Wang (王旭),[1] and Jifu Zhou (周济福)[1,2,a)]

## AFFILIATIONS

[1]Laboratory for Mechanics in Fluid Solid Coupling Systems, Institute of Mechanics, Chinese Academy of Sciences, Beijing 100190, China
[2]School of Engineering Sciences, University of Chinese Academy of Sciences, Beijing 100049, China

[a)]Author to whom correspondence should be addressed: zhoujf@imech.ac.cn

## ABSTRACT

Deep-sea mining lifting risers experience vibrations induced by the action of ocean waves and currents, and these vibrations have an impact on the lifting efficiency of ores transported inside the risers. Here, to investigate the effect of riser vibration on ore transport, the motion of a single solid particle in a riser oscillating in the lateral direction is simulated taking account of collisions between the particle and the riser using the governing equation for motion of a spherical particle in Poiseuille flow and the Hertz–Mindlin soft sphere collision model. Validations are conducted based on comparisons between numerical and experimental results. Then, the motion of the particle in the vibrating riser is explored, considering the effects of the initial position of release of the particle, the frequency and amplitude of the riser vibrations, and collisions between the particle and the riser. It is found that the initial position of release affects only the initial motion of the particle, but not its overall motion. With increasing vibrational frequency and amplitude of the riser, the relative lateral velocity of the particle shows an increasing trend, while its vertical velocity and lifting distance are clearly decreased. The frequency with which the vertical particle velocity varies is twice as the vibrational frequency of the riser. Moreover, collisions have significant effects on the particle motion, especially on the velocities of the particle, the phase difference between the displacements of the particle and the vibrating riser, and the particle trajectory. Finally, the behavioral regime map of the particle under different vibrational frequencies and amplitudes of the riser is established preliminarily.





## I. INTRODUCTION

In deep-sea mining, the manganese nodules estimated to be in the range of tens of centimeters are first collected in a chamber by collectors, and then crushed into centimeter-sized particles by a crusher, and finally transported through the riser. Many issues need to be addressed here due to the complexity of the deep-sea mining process. For example, apart from the ores and seawater, a small amount of air might exist in the lifting riser, and thus, the gas–liquid flow may exist in the process of deep-sea mining, which has been investigated systematically and detailed by some scholars.[1–4] Moreover, lifting risers exhibit complicated dynamical behavior when they are subjected to waves and currents. A number of scholars have conducted studies on this issue,[5–9] and notably, Li *et al.*[8,9] introduced a linear-time-invariance notion to the Koopman analysis, offering a fresh perspective on the study of fluid–structure interaction and nonlinear, stochastic systems. However, limited attention has been given to the characteristics of the motion of ores in lifting risers, which is one of the most important tasks required to guarantee the safety of deep-sea mining operations. Dynamic responses, such as vortex-induced vibration, can be induced when lifting risers with a large aspect ratio are subjected to wave and current loads. These riser oscillations can cause collisions between the ore and the inner wall of the riser, and such collisions will have a significant impact on the motion of the ore. Since the security and efficiency of deep-sea mining depend strongly on the conveyance of ores in lifting risers, it is of great importance to consider the effect of riser vibration on ore motion.

The dynamics of both a single particle and multiple particles moving in fluids have been studied extensively for many years. For example, from an analysis of a rotating sphere in a fluid, Magnus[10] found that a force, subsequently termed the Magnus force,[11] was exerted upon the sphere. A particle accelerating in a fluid is subjected to two kinds of force: the added-mass force and the Basset force related to viscous effects. Basset[12] obtained an expression for the latter force that is valid when a spherical particle is moving at low velocity but with rapid acceleration. Odar and Hamilton[13] obtained a more general expression for the two forces involving the added-mass coefficient $C_A$,

an experimentally determined coefficient $C_H$, the acceleration number $A_c$ (a dimensionless ratio related to the velocity, acceleration, and diameter of the sphere), and the Reynolds number *Re*. Michaelides and co-workers[14–16] compared the Basset force with the total force on a particle in the case of turbulent flow in a tube and found that the Basset force term could be ignored in the equation of motion of the particle when the particle diameter was larger than 1 $\mu$m, the dimensionless frequency of variation was less than 0.5, and the fluid-to-particle density ratio was less than 0.002 or greater than 0.7.

Based on earlier work, an equation for the motion of a sphere in nonuniform flow was first proposed by Tchen.[17] This equation was later modified and applied by many researchers.[18–22] Using the particle equation of motion and the Navier–Stokes equation, Feng *et al.*[23,24] studied the sedimentation of a circular particle in a vertical channel in two dimensions and discovered five different regimes of motion as the Reynolds number was increased to 600: steady motion with and without overshoot and weak, strong, and irregular oscillations. The transitions between adjacent regimes of motion arising from variations in the solid/fluid density ratio have been discussed by Jenny *et al.*[25] in terms of primary and second bifurcations. The effects of the Reynolds number, particle–tube size ratio, and degrees of freedom on the trajectory and velocity of a particle falling in a fluid-filled tube, as well as on the associated vortex structures, have been analyzed and discussed by a number of authors.[26–28]

Particles in a shear flow behave very differently compared with those in still water, and hence, the motion of rigid spheres in linear shear flow and Poiseuille flow have attracted much attention. In the case of particles in Poiseuille flow in a vertical tube, it was observed experimentally by Oliver[29] that downward-settling particles in downward-flowing liquid moved toward the wall, whereas upward-settling particles moved toward the axis, and this behavior was also shown theoretically by Saffman[30,31] and by Moore and Saffman.[32] Particles suspended in a tube flow with relatively low concentration were found by Segré and Silberberg,[33] Matas *et al.*,[34] and Pan *et al.*[35] to accumulate at a position approximately one-third of the tube radius away from the tube wall. The distribution of neutrally buoyant spherical particles in circular tube flow was measured by Morita *et al.*,[36] who found two peaks in the radial probability function, corresponding to two annuli at which particles accumulated. The inertial focusing of an isolated particle and of a dilute suspension of particles in wall-bounded laminar flow was studied numerically by Nakayama *et al.*[37] and Aouane *et al.*[38] It was observed that there are three *Re* regimes of particle-focusing patterns and the channel focusing length increases with *Re* for $Re \leq 600$. The trajectories, velocities, and equilibrium positions of a neutrally buoyant sphere in vertical and horizontal channels were investigated by Fox *et al.*[39] The lift and drag forces acting on a spherical particle in a linear shear flow bounded by a single wall were examined by Shi and Rzehak[40] and by Ekanayake *et al.*,[41] with particular attention being paid to the particle migration caused by hydrodynamic lift forces. In addition to the above-mentioned studies, the laws of motion of single and multiple particles in fluid flows have been widely investigated both experimentally and theoretically.[42–48]

The studies of particles moving in shear flow described above were concerned mainly with the case of low Reynolds number, in which the density of particles was approximately equal to that of the fluid or the particle diameter was very small. However, the more general case of particles with a large density difference from the fluid has also been studied. The lateral migration and the equilibrium position of non-neutrally buoyant particles in planar Poiseuille flow and Couette flow were investigated by Feng *et al.*[24] and Fox *et al.*[39] It was found that when the density difference between particle and fluid is large enough, the equilibrium position of the particle shifts toward the centerline of the riser regardless of whether the particle is lighter or heavier than the fluid. It should be noted that the findings of these two studies were different from the predictions of the perturbation theory of Vasseur and Cox.[49] The trajectories of a sphere in Poiseuille flow with $Re_t = 20–150$ ($Re_t$ is the Reynolds number of the tube) were simulated by Shao *et al.*[50] for various density ratios $\rho_r = \rho_p/\rho_f$ ($\rho_p$ and $\rho_f$ are the densities of the particle and the fluid, respectively) and diameter ratios $\lambda_a = d/D$, and the results obtained were found to be the same as those of Feng *et al.*[24] when the particle was heavier than the ambient fluid. The migration of particles was studied by Shao *et al.*,[50] Matas *et al.*,[34,51,52] and Bai *et al.*[53] for various particle–tube size ratios and Reynolds numbers. Liu *et al.*[54] carried out simulations to investigate the behavior of the hydrodynamic forces and the velocity of a heavy sphere in upward Poiseuille flow for a wide range of density ratios $1.1 \leq \rho_r \leq 4$ and various degrees of freedom. The above-mentioned studies have provided a clear picture of the motion of particles in a stationary riser with upward Poiseuille flow.

In the previous studies described above, the motion of particles in fluid contained in a fixed pipe has mainly been investigated without taking account of any movement of the pipe. However, as mentioned at the start of this section, lifting risers can move or oscillate periodically when subjected to waves and currents in the ocean. Once such oscillations occur, collisions between particles and riser are inevitable, and these can intensify the dynamic motion of the particles. Thus, it is necessary to investigate the motion of particles in fluid contained in a vibrating riser and the underlying mechanisms. Undoubtedly, in the study of this issue, particles' motion and their interactions can be affected by the particle count, which has been studied by numerous scholars.[55–60] However, it should be noticed that the underlying mechanisms behind the occurrence of these phenomena are extremely complicated with the increase in particle count, which has received limited attention. Therefore, it is informative to explore the motion of a single particle within a vibrating riser first, as it can be a foundation for the investigation of the multiparticle behaviors within such riser.

Additionally, ores transported in the riser might be irregular, and according to the investigation of Chen *et al.*,[61] it is found that irregularly shaped particles, compared to spherical particles, can increase the possibility of blockage, and the particle behavior varies with different parameters. However, previous research works on the behaviors of ores in a deep-sea vertical riser (stationary riser) regarded such ores as spheres, as investigated by Liu *et al.*,[54] Ren *et al.*,[57] Wan *et al.*,[58] and Zhang *et al.*[62] Therefore, simplifying the shape of the ore to a sphere provides a convenient and effective approach to analyze the behavior of ores. Accordingly, in our study, the ore and the lifting riser are simplified as a spherical particle and a vertical riser, respectively. Thus, the problem reduces to that of a single spherical particle moving in a riser with transverse vibration.

Based on the above simplification, here, the motion of a single particle in a transversely oscillating riser is investigated using the governing equation for the motion of a sphere together with the Hertz–Mindlin soft sphere collision model,[63] and the internal flow in the riser is taken to be upward Poiseuille flow. First, the model

established using this approach is validated through a comparison of numerical results and experimental data. Then, the characteristics of particle motion, such as velocities and trajectories, are analyzed and discussed when positions of initial particle release, vibrational frequencies, and amplitudes of the riser are changed. The effect on particle motion of collisions between the particle and the oscillating riser is also investigated. It should be emphasized here that the aim of this study is to carry out a preliminary exploration of the characteristics of motion of a single particle in an oscillating riser that will provide a foundation for further experimental and numerical investigations of the motion of multiple particles in which additional factors are taken into account.

The remainder of the paper is structured as follows. The equation governing the motion of the sphere and the model adopted for collisions between the particle and the vibrating riser are introduced in Sec. II. Section III presents a validation of the model based on a comparison between numerical and experimental results. Then, in Sec. IV, the effects on particle motion of the position at which the particle is initially released, the vibrational amplitude and frequency of the riser, and the particle–riser collisions are analyzed and discussed. Moreover, the possible behavioral regimes of the particle affected by the vibrational frequency and amplitude of the riser are summarized and depicted in Sec. IV D. Finally, the conclusions of the study are drawn in Sec. V.

## II. NUMERICAL MODEL

### A. Governing equations of particle motion

As mentioned above, the ore in the vibrating riser is simplified as a spherical particle. In addition, particle rotation and fracture of the particle during collisions are left out of consideration. In addition, in order to give prominence to the influence of the collision between the particle and the riser on the motion of the particle inside a vibrating riser, the perturbation on the flow field by the particle is not taken into consideration in the present study and hence, the flow velocity inside the riser is given as was done by some researchers such as Maxey and Riley[19] and Michaelides and co-workers.[14–16]

The particle moving in the vibrating riser is subject to gravitational, impact, and fluid forces. The drag force, Saffman lift force, pressure gradient force, additional forces, and Basset force are included the fluid force exerted on the particle. When a collision occurs between the particle and the oscillating riser, the collision force must be taken into account, which will be done in Sec. II B. The governing equation for the spherical particle moving in the fluid is given as[22]

$$\begin{aligned}\frac{\pi d^2}{6}\rho_p\frac{d\mathbf{v}_{pi}}{dt} &= \frac{\pi d^2}{8}\rho_f C_D|\mathbf{u}_{fi}-\mathbf{v}_{pi}|(\mathbf{u}_{fi}-\mathbf{v}_{pi}) + \frac{\pi d^3}{12}\rho_f\left(\frac{d\mathbf{v}_{pi}}{dt}-\frac{d\mathbf{u}_{fi}}{dt}\right)\\ &+\frac{\pi d^3}{6}(\rho_p-\rho_f)\mathbf{g}_i + \frac{\pi d^3}{8}\rho_f C_{LS}(\mathbf{u}_{fi}-\mathbf{v}_{pi})\times 2\boldsymbol{\omega}_{fi}\\ &+C_H\frac{d^2}{4}\sqrt{\pi\rho_f\mu_f}\int_0^t\frac{d(\mathbf{u}_{fi}-\mathbf{v}_{pi})}{d\tau}\frac{d\tau}{\sqrt{t-\tau}}\\ &+\frac{\pi d^3}{6}\rho_f\left(\frac{D\mathbf{u}_{fi}}{Dt}-\frac{\mu}{\rho_f}\nabla^2\mathbf{u}_{fi}\right)\\ &= F_D+F_{AM}+F_{G-B}+F_{LS}+F_H+F_{FS}, \end{aligned}\tag{1}$$

where the various terms on the right-hand side of Eq. (1) are as follows: $F_D$ denotes the drag force; $F_{AM}$ is the force due to the added mass; $F_{G\text{-}B}$ is the body force (gravity minus buoyance); $F_{LS}$ represents the Saffman force resulting from the shear of the fluid; $F_H$ is the Basset force in the time domain, representing the memory effect on the particle motion; and the last term, $F_{FS}$, denotes the force of fluid stress gradients on the particle, which results from the acceleration of the local fluid element or the stress on the sphere owing to the undisturbed fluid flow. In addition, $d$ is the diameter of the spherical particle, $\rho_p$ and $\rho_f$ are the densities of the particle and the fluid, respectively, $\mathbf{u}_{fi}$ and $\mathbf{v}_{pi}$ are the particle and fluid velocities, respectively, and $\boldsymbol{\omega}_{fi}=\frac{1}{2}\nabla\times\mathbf{u}_{fi}$ is the fluid vorticity. $\mu$ denotes the dynamic viscosity of the fluid. $C_D$, $C_{LS}$, and $C_H$ are the drag coefficient, Saffman lift coefficient, and Basset term (history term) coefficient, respectively. Here, the fluid density $\rho_f$, vertical velocity $u_{cm}$, and riser diameter $D$ are taken as dimensional units. The corresponding dimensionless quantities can be obtained as follows:

$$\mathbf{v}^*_{pi}=\frac{\mathbf{v}_{pi}}{u_{cm}},\quad \mathbf{u}^*_{fi}=\frac{\mathbf{u}_{fi}}{u_{cm}},\quad \boldsymbol{\omega}^*_{fi}=\frac{\boldsymbol{\omega}_{fi}}{u_{cm}/D},\quad Fr=\frac{|\mathbf{g}_i|D}{u_{cm}^2},$$
$$Re_{cm}=\frac{\rho_f u_{cm}D}{\mu},\quad \frac{\rho_f u_{cm}D}{\mu},\quad \beta=\frac{\rho_p}{\rho_f},\quad \lambda=\frac{1}{1+0.5\beta}.$$

The governing equation can then be expressed in a dimensionless form as

$$\frac{d\mathbf{v}^*_{pi}}{dt}=\lambda\left[\begin{aligned}&\frac{3}{4}C_D|\mathbf{u}^*_{fi}-\mathbf{v}^*_{pi}|\left(\mathbf{u}^*_{fi}-\mathbf{v}^*_{pi}\right)+\frac{1}{2}\frac{d\mathbf{u}^*_{fi}}{dt}\\ &+(1-\beta)Fr\frac{\mathbf{g}_i}{|\mathbf{g}_i|}+\frac{3}{4}C_{LS}\left(\mathbf{u}^*_{fi}-\mathbf{v}^*_{pi}\right)\times 2\boldsymbol{\omega}^*_{fi}\\ &+\frac{3}{12}C_H\sqrt{\frac{\pi}{Re_{cm}}}\int_0^{t^*}\frac{d(\mathbf{u}^*_{fi}-\mathbf{v}^*_{pi})}{d\tau^*}\frac{d\tau^*}{\sqrt{t^*-\tau^*}}\\ &+\frac{D\mathbf{u}^*_{fi}}{Dt}-\frac{1}{Re_{cm}}\nabla^{*2}\mathbf{u}^*_{fi}\end{aligned}\right].\tag{2}$$

In comparison with the other terms, $Re_{cm}^{-1}\nabla^{*2}\mathbf{u}^*_{fi}$ can be ignored, since $Re_{cm}$ is generally of the order of magnitude of $10^5$. Henceforth, for brevity, the superscript $*$ will be omitted. Finally, the governing equation is expressed as

$$\frac{d\mathbf{v}_{pi}}{dt}=\lambda\left[\begin{aligned}&\frac{3}{4}C_D|\mathbf{u}_{fi}-\mathbf{v}_{pi}|(\mathbf{u}_{fi}-\mathbf{v}_{pi})+\frac{1}{2}\frac{d\mathbf{u}_{fi}}{dt}+(1-\beta)Fr\frac{\mathbf{g}_i}{|\mathbf{g}_i|}\\ &+\frac{3}{4}C_{LS}(\mathbf{u}_{fi}-\mathbf{v}_{pi})\times 2\boldsymbol{\omega}_{fi}\\ &+\frac{3}{12}C_H\sqrt{\frac{\pi}{Re_{cm}}}\int_0^{t}\frac{d(\mathbf{u}_{fi}-\mathbf{v}_{pi})}{d\tau}\frac{d\tau}{\sqrt{t-\tau}}+\frac{D\mathbf{u}_{fi}}{Dt}\end{aligned}\right].\tag{3}$$

As described by Clift *et al.*,[64] $C_D$ and $C_{LS}$ are the drag coefficient and Saffman lift coefficient, which depend on the Reynolds number $Re_p$ and the shear Reynolds number $Re_{\text{shear}}$ of the particle,

$$Re_p=\frac{\rho_f d\sqrt{|\mathbf{u}_{fi}-\mathbf{v}_{pi}|^2}}{\mu},\tag{4}$$

$$C_{LS} = \frac{4.1126}{\sqrt{Re_{\text{shear}}}} f(Re_p, Re_{\text{shear}}), \quad Re_{\text{shear}} = \frac{\rho_f d^2 |\nabla \times \mathbf{u}_{fi}|}{\mu_f}, \tag{5}$$

$$f(Re_p, Re_{\text{shear}}) = \begin{cases} \left(1 - 0.3314\sqrt{\frac{Re_{\text{shear}}}{2Re_p}}\right) e^{-0.1Re_p} \\ \quad +0.3314\sqrt{\frac{Re_{\text{shear}}}{2Re_p}}, & Re_p \le 40, \\ 0.0524\sqrt{0.5Re_{\text{shear}}}, & Re_p > 40. \end{cases} \tag{6}$$

The drag coefficient $C_D$ of an unbounded flow field depends closely on the Reynolds number. In addition, the diameter ratio $\alpha = d/D$ also plays an important role in determining $C_D$ when the particle moves in the riser.[64] After correction, $C_D$ can be expressed as follows:

$$C_D = \begin{cases} \frac{24}{Re_p} K, & Re_p \le 1, \\ \frac{24}{Re_p}\left(\frac{1}{6} Re_p^{2/3} + K\right), & 1 < Re_p < 100, \\ 0.42K_{F1}, & 100 < Re_p < 600, \\ 0.42K_{F2}, & Re_p > 10^5, \end{cases} \tag{7}$$

where

$$K = \frac{1 - 0.75857\alpha^5}{1 - 2.1050\alpha + 2.0865\alpha^3 - 1.7068\alpha^5 + 0.72603\alpha^6}, \tag{8}$$

$$K_{F1} = \frac{1}{1 - 1.6\alpha^{1.6}}, \tag{9}$$

$$K_{F2} = \frac{1 + 1.45\alpha^{4.5}}{(1 - \alpha^2)^2}. \tag{10}$$

As investigated by Michaelides and Roig,[65] the empirical coefficient of Basset term $C_H$ depends on the Reynolds number of the particle $Re_p$ and Strouhal number $St$. The expressions of $C_H$ and $St$ are shown as follows:

$$St = \frac{9\mu}{16\pi f R_p^2 \rho_f}, \tag{11}$$

$$C_H = 6.00 - 3.16\left[1 - \exp\left(-0.14Re_p St^{0.82}\right)^{2.5}\right], \tag{12}$$

where $f$ is the frequency of the fluid oscillations. $R_p$ denotes the sphere radius.

### B. Collision model

As collisions will occur between the particle and the vibrating riser, it is necessary to take the effect of these collisions on particle motion into account during the calculation. Two collision models can be employed for simulating particle-wall collisions, namely, hard sphere model[66] and soft sphere model.[63] The former enables the calculation of post-collision velocities, but it fails to capture variations in particle velocities during collisions. However, the soft sphere model addresses this limitation. Therefore, the Hertz–Mindlin soft sphere collision model is selected for this purpose, and the solid particles in the ore-lifting riser are assumed to be ideal soft spheres during our investigation. In this collision model, the overlap distance $\delta$ is solved each time step during collision to calculate the collision force $\mathbf{F}_{\text{col}}$ and particle velocity. Since the overlap distance $\delta$, consisting of the normal overlap distance $\delta_n$ and tangential overlap distance $\delta_\tau$, varies with time, the trend of variation of the particle velocity can be obtained, enabling analysis of the influence of collisions on particle motion. The collision force $\mathbf{F}_{\text{col}}$ can be expressed as

$$\mathbf{F}_{\text{col}} = \mathbf{F}_n + \mathbf{F}_\tau, \tag{13}$$

where $\mathbf{F}_n$ and $\mathbf{F}_\tau$ denote the normal and tangential forces, respectively. These forces can be calculated as

$$\mathbf{F}_n = \left(k_n |\delta_n|^{3/2} - N_n \mathbf{U}_{pw} \cdot \mathbf{n}\right)\mathbf{n}, \tag{14}$$

$$\mathbf{F}_\tau = \begin{cases} -\mu_f |k_n \delta_n| \frac{\delta_\tau}{|\delta_\tau|} \boldsymbol{\tau}, & k_\tau |\delta_\tau| > \mu_f |k_n \delta_n|, \\ -k_\tau \delta_\tau \boldsymbol{\tau} - N_\tau \mathbf{U}_{pw,\tau}, & k_\tau |\delta_\tau| \le \mu_f |\mathbf{F}_n|, \end{cases} \tag{15}$$

with

$$\mathbf{U}_{pw,\tau} = \mathbf{U}_{pw} - (\mathbf{U}_{pw} \cdot \mathbf{n})\mathbf{n} - (R_p \boldsymbol{\omega}_p + R_w \boldsymbol{\omega}_w) \times \mathbf{n}, \tag{16}$$

$$\mathbf{n} = \frac{\mathbf{P}_{\text{axis}} - \mathbf{P}_p}{|\mathbf{P}_{\text{axis}} - \mathbf{P}_p|}, \tag{17}$$

where $k_n$ and $k_\tau$ are the normal and tangential elastic constants, $\delta_n$ and $\delta_\tau$ are the normal and tangential overlap distance, and $N_n$ and $N_\tau$ are the normal and tangential damping constants (usually, $N_n = N_\tau$). The relative velocity can be calculated as $\mathbf{U}_{pw} = \mathbf{U}_p - \mathbf{U}_w$, where $\mathbf{U}_p$ and $\mathbf{U}_w$ are the velocities of the particle center and vibrating riser, respectively. $\mathbf{U}_{pw,\tau}$ represents the tangential component of the relative speed of the contact point between the particle and riser wall. The normal unit vector $\mathbf{n}$ and normal overlap distance $\delta_n$ are defined in terms of the positions of the particle center $\mathbf{P}_p(x_p, y_p)$ and riser centerline $\mathbf{P}_{\text{axis}}(x_c, y_c)$. $\boldsymbol{\tau}$ represents the tangential unit vector. In addition, $k_n$, $k_\tau$, $N_n$, $\delta_n$, and $\delta_\tau$ are set as follows:

$$k_n = \frac{4}{3} E_{\text{eq}} \sqrt{R_{\text{eq}}}, \tag{18}$$

$$k_\tau = 8G_{\text{eq}} \sqrt{R_{\text{eq}} \delta_n}, \tag{19}$$

$$N_n = C_{n,rest} \delta_n^{1/4} \sqrt{k_n M_{eq}}, \tag{20}$$

$$\delta_n = R_p + R_w - |\mathbf{P}_p - \mathbf{P}_w|, \tag{21}$$

$$\delta_\tau = |\mathbf{U}_{pw,\tau}| \Delta t, \tag{22}$$

where $R_p$ is the particle radius, $C_{n,rest}$ is the normal recovery coefficient, and $\Delta t$ is the time step. The subscript "$eq$" indicates the equivalent parameters that are used because of the different material parameters of the particle and riser. The equivalent Young's modulus $E_{eq}$, equivalent radius $R_{eq}$, equivalent mass $M_{eq}$, and equivalent shear modulus $G_{eq}$ are defined as follows:

$$E_{eq} = \left(\frac{1 - \upsilon_p^2}{E_p} + \frac{1 - \upsilon_w^2}{E_w}\right)^{-1}, \tag{23}$$

$$G_{eq} = \left[\frac{2\left(2 + \upsilon_p - \upsilon_p^2\right)}{E_p} + \frac{2\left(2 + \upsilon_w - \upsilon_w^2\right)}{E_w}\right]^{-1}, \tag{24}$$

$$R_{eq} = \left(\frac{1}{R_p} + \frac{1}{R_w}\right)^{-1}, \tag{25}$$

$$M_{eq} = \left(\frac{1}{M_p} + \frac{1}{M_w}\right)^{-1}, \tag{26}$$

where subscripts $p$ and $w$ represent particle and riser wall. $E$, $G$, $M$, and $R$ are the Young's modulus, shear modulus, mass, and radius. In the case of particle–wall collision, the riser wall is regarded as a particle with infinite radius $R_w = \infty$ and mass $M_w = \infty$, and thus, $R_{eq} = R_p$ and $M_{eq} = M_p$.

Since a particle–riser collision occurs in three dimensions, the relative velocity of the particle can be decomposed into three components: two in the tangential directions and one in the normal direction. As shown in Fig. 1, the normal and tangential relative velocities can be expressed in terms of the velocity difference and the angle $\theta$ between the particle and the riser in the plane perpendicular to the riser centerline,

$$\theta = \arctan\left(\frac{y_p - y_c}{x_p - x_c}\right), \tag{27}$$

$$\begin{cases} v_n = (v_{py} - u_{cy})\sin\theta + (v_{px} - u_{cx})\cos\theta, \\ v_{\tau\theta} = (v_{py} - u_{cy})\cos\theta + (v_{px} - u_{cx})\sin\theta, \\ v_{\tau z} = v_{pz}. \end{cases} \tag{28}$$

The directions of the normal relative velocity $v_n$ and tangential relative velocity $v_{\tau\theta}$ are set along the radial and one of the tangential directions of the riser, respectively, as shown in Fig. 1. The other tangential direction $v_{\tau z}$ is set along the centerline of the riser (the $z$ axis).

Whether a collision occurs depends on the distance between the particle center and the riser centerline, which can be denoted by $h = \sqrt{(x_p - x_c)^2 + (y_p - y_c)^2}$, where the cross section of the riser is in the $x$–$y$ plane. The $z$ axis corresponds to the vertical centerline of the riser. $(x_p, y_p)$ and $(x_c, y_c)$ are the coordinates of the particle center and the riser centerline. A collision between the particle and the oscillating riser will occur when $h > (D - d)/2 - \varepsilon d$, where $h$ is the distance between the particle center and the riser centerline, and $\varepsilon$ is a tolerance coefficient ($\varepsilon = 10^{-3}$–$10^{-4}$ in this study). The collision between particle and riser stops when the normal overlap distance $\delta_n \le 0$.

### C. Detailed description of the solving procedure

The particle motion in a vibrating riser can be calculated using governing equations of particle motion and collision model, as described in Secs. II A and II B. Here, the conjunctional solution procedure for these two equations is presented in detail.

The solve processor of the collision model in conjunction with Eq. (3) is presented in Fig. 2. During the calculation, the initial position and velocity of the particle are set as $(x_{p0}, y_{p0}, z_{p0})$ and $(v_{px0}, v_{py0}, v_{pz0})$, respectively. Before iteratively solving for particle velocities, it is necessary to determine whether a collision between the particle and the riser wall occurs. The distance between the particle center and the riser centerline is denoted by $h = \sqrt{(x_p - x_c)^2 + (y_p - y_c)^2}$, where the cross section of the riser is located in the $x$–$y$ plane.

(1) When $h > (D - d)/2 - \varepsilon d$, the collision occurs, and the particle velocities are determined using the Hertz–Mindlin soft sphere collision model described in Sec. II B in the revised manuscript. The special processor of the collision can be expressed as follows:
   (a) Before the collision, the positions and velocities of particle and riser wall are represented as $[x_p^{(0)}, y_p^{(0)}, z_p^{(0)}]$, $[v_{px}^{(0)}, v_{py}^{(0)}, v_{pz}^{(0)}]$ and $[x_c^{(0)}, y_c^{(0)}, z_c^{(0)}]$, $[u_{cx}^{(0)}, u_{cy}^{(0)}, u_{cz}^{(0)}]$, respectively. It should be pointed out that the relative velocity of the particle to the riser wall is required for solving the collision. The relative velocity before the collision is

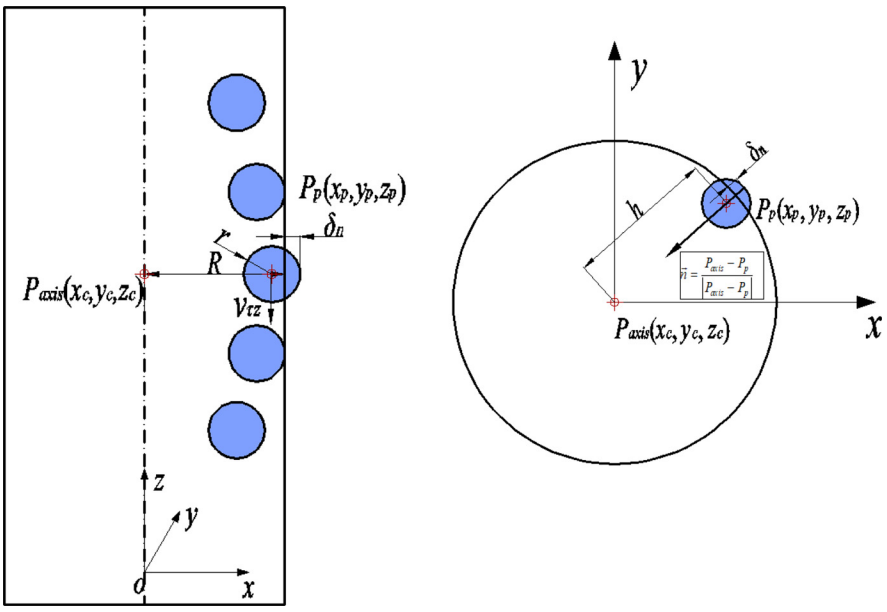


**FIG. 1.** Schematic representation of the model of a collision between the particle and the riser wall.

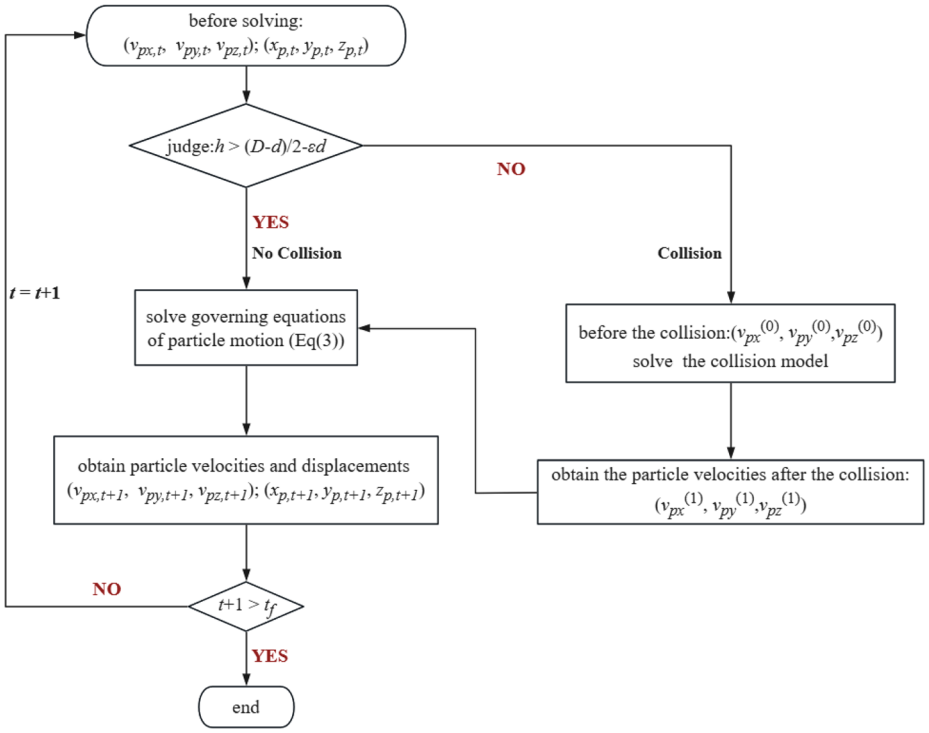


**FIG. 2.** A flow chart showing solving procedure of the coupling method.

calculated by $[v_{pxre}^{(0)}, v_{pyre}^{(0)}, v_{pzre}^{(0)}] = [v_{px}^{(0)} - u_{cx}^{(0)}, v_{py}^{(0)} - u_{cy}^{(0)}, v_{pz}^{(0)} - u_{cz}^{(0)}]$. In addition, since a particle-riser collision occurs in three dimensions, the relative velocity of the particle can be decomposed into three components: two in the tangential directions and one in the normal direction. As shown in Fig. 1, the normal and tangential relative velocities can be expressed in terms of the velocity difference and the angle $\theta$ between the particle and the riser in the plane perpendicular to the riser centerline is expressed in Eq. (27).

Therefore, at the beginning of the collision, the normal and tangential velocities can be expressed as

$$\begin{cases} v_n^{(0)} = v_{pxre}^{(0)} \cos\theta + v_{pyre}^{(0)} \sin\theta, \\ v_{\tau\theta}^{(0)} = v_{pxre}^{(0)} \sin\theta + v_{pyre}^{(0)} \cos\theta, \\ v_{\tau z}^{(0)} = v_{pzre}^{(0)}. \end{cases} \tag{29}$$

The collision forces in normal and tangential directions are calculated as Eqs. (14) and (15). It should be noted that at the beginning of the collision, the overlap is set as 0, and so the collision forces $F_n^{(0)}$ and $F_\tau^{(0)}$ are equal to 0, indicating zero acceleration for the particle. However, due to the existence of the relative velocity, the particle keeps moving toward the wall and the overlap exists. Consequently, the collision process can be progressed.

(b) As the collision progresses, the overlap distances and velocities in normal and tangential directions can be obtained by the following equations:

$$\delta_n(i) = \delta_n(i-1) + v_n(i-1)\Delta t + 0.5a_n(i-1)\Delta t^2, \tag{30}$$

$$\delta_\tau(i) = \delta_\tau(i-1) + v_\tau(i-1)\Delta t + 0.5a_\tau(i-1)\Delta t^2, \tag{31}$$

where $\Delta t$ and $i$ represent the time step and the number of the time steps, respectively. The accelerations of the relative motion between the particle and the riser wall in the normal and tangential directions are set as $a_n$ and $a_\tau$. "$(i)$" and "$(i-1)$" denote the variables of this and previous time step, respectively. The forces $F_n$ and $F_\tau$ at this time step can be obtained using the overlap distance $\delta_n(i)$ and $\delta_\tau(i)$, and therefore, the acceleration at this time step $i$ can be calculated by the following expressions:

$$a_n(i) = F_n(i)/m_p \quad a_\tau(i) = F_\tau(i)/m_p. \tag{32}$$

The relative velocities at the next time step $i+1$ can be obtained by

$$v_n(i+1) = v_n(i) + a_n(i)\Delta t, \tag{33}$$

$$v_\tau(i+1) = v_\tau(i) + a_\tau(i)\Delta t. \tag{34}$$

After completing the calculations within a time step $\Delta t$, the process continues to be repeated if the condition $d_n(i) \geq 0$ is satisfied. When $d_n(i) \geq 0$ but $d_\tau(i) < 0$, the overlap distance and relative velocities in the normal direction are still obtained using the procedure described above. Meanwhile, the variables in the tangential direction will not change as the time step progresses, meaning that they remain the same as those in the previous time step, denoted as "$^*(i+1) = {}^*(i)$," where "$^*$" denotes the variables during the collision calculation. Finally, as $d_n(i) < 0$,

the loop process mentioned above is terminated. At this moment, the relative velocities after collision are denoted as $v_n$(end), $v_{t\theta}$(end), and $v_{tz}$(end), where "end" represents the last time step of the collision.

(c) For convenience of calculation, the velocities after the collision are converted to the Cartesian coordinate and expressed as

$$\begin{cases} v_{px}^{(1)} = v_n(\text{end})\cos\theta + v_{\tau\theta}(\text{end})\sin\theta + u_{cx}^{(0)}, \\ v_{py}^{(1)} = v_n(\text{end})\sin\theta - v_{\tau\theta}(\text{end})\cos\theta + u_{cy}^{(0)}, \\ v_{\tau z}^{(1)} = v_{pz}(\text{end}) + u_{cz}^{(0)}, \end{cases} \tag{35}$$

wherein superscript "(1)" represents the variables of the particle after the collision. In addition, it should be noted that the positions of particle and riser axis remain the same $\{[x_p^{(1)}, y_p^{(1)}, z_p^{(1)}] = [x_p^{(0)}, y_p^{(0)}, z_p^{(0)}], [x_c^{(1)}, y_c^{(1)}, z_c^{(1)}] = [x_c^{(0)}, y_c^{(0)}, z_c^{(0)}]\}$ before and after the collision due to that the duration of collision is transient, but an abrupt in velocities exists.

(d) After the collision, the particle velocity can be obtained using the governing equation expressed as Eq. (3). The fourth–fifth order Runge–Kutta algorithm is employed to solve Eq. (3). During the calculation, the time step for the fluid is chosen to be $10^{-3}$, meaning that the variables of the particle and fluid are updated every $10^{-3}$ unit of time. The time step for the collisions process is set as $10^{-6}$, which is significantly smaller compared to the time step for the fluid, allowing for a more accurate calculation of the particle collisions.

(2) When $h \le (D - d)/2 - \varepsilon d$, collisions do not occur, and the variation of the particle velocity with time can be determined by solving Eq. (3) iteratively, as shown in (d).

### D. Dimensionless parameters of particle motion

The motion of the sphere in the vibrating riser is mainly affected by the fluid force and gravitational force when the fluid in the riser is set as upward Poiseuille flow. Collisions between the particle and riser wall will occur owing to the vibration of the riser. As noted above, the occurrence of a collision depends on the distance between the particle center and the riser centerline, $h = \sqrt{(x_p - x_c)^2 + (y_p - y_c)^2}$. The parameters associated with the distance $h$ are the riser diameter $D$, the fluid density $\rho_f$, the fluid viscosity $\mu$, the maximum vertical velocity $u_{cm}$, the particle diameter $d$, the particle density $\rho_p$, the gravitational acceleration $g$, and the position $P_0(x_{p0}, y_{p0})$ at which the particle is initially released. The vibrational amplitude $A_m$ and frequency $\omega$ of the riser must also be considered here. We, thus, have the following functional relationship:

$$h = f\left(D, \rho_f, \mu, u_{cm}; d, \rho_p; g; A_m, \omega; P_0\right). \tag{36}$$

The fluid density $\rho_f$, riser diameter $D$, and maximum vertical velocity $u_{cm}$ are selected as dimensional units. Equation (36), then, becomes

$$\frac{h}{D} = f\left(\frac{\rho_f u_{cm} D}{\mu}; \frac{d}{D}, \frac{\rho_p}{\rho_f}; \frac{g}{u_{cm}^2/D}; \frac{A_m}{D}, \frac{\omega}{u_{cm}/D}; \frac{P_0}{D}\right). \tag{37}$$

Here, seven dimensionless parameters appear to be related to $h$. In our simulation, we have $\rho_f = 1000\,\text{kg/m}^3$, $\mu = 0.001$ Pa s, $g = 9.8$ m/s$^2$, $u_{cm} = 1$ m/s, $\rho_P = 2000\,\text{kg/m}^3$, $d = 0.01$ m, and $D = 0.1$ m. Thus, $\rho_f u_{cm} D/\mu$, $d/D$, $\rho_p/\rho_f$, and $g/(u_{cm}^2/D)$ are constants. Consequently, the motion of the particle is mainly determined by $A_m/D$, $\omega/(u_{cm}/D)$, and $P_0/D$. In the following analysis of a particle moving in a vibrating riser with upward Poiseuille, the effects of these parameters are mainly considered.

## III. VALIDATION

Before the implementation of our model for further investigations, we shall validate it by comparison with existing results published by Gondret *et al.*[67]

We first consider the experiment conducted by Gondret *et al.*,[67] which investigated the behavior of a steel particle falling in fluid and colliding with the bottom of a vessel. The collision between the particle and the vessel bottom is simulated using the soft collision model presented in Sec. II B, with the particle velocity being calculated from Eq. (3).

In the experiment by Gondret *et al.*,[67] the steel sphere had a diameter of 3 mm and a density of $\rho_p = 7800\,\text{kg/m}^3$. The vessel was filled with silicone oil of density $\rho_f = 935\,\text{kg/m}^3$ and viscosity $\mu = 0.01$ Pa s. The particle velocity and displacement are calculated with and without the Basset force. Comparisons of the calculated data with the experimental results are shown in Fig. 3, in which $h$ represents the distance between the lowest point of the sphere and the bottom wall of the vessel. $t = 0$ is defined as the time at which the first collision occurs.

It can be seen that the numerical results show better agreement with the experimental data. For the particle velocity and displacement, there is an error of approximately 5% before and after each collision. As noted by Gondret *et al.*,[67] there was the possibility of errors in measuring the sphere position and velocity as well as the time interval between two successive images during the experiments, and these might account for these discrepancies between the numerical and experimental results. In addition, fluid dissipation will also contribute to such errors. However, it should be emphasized that the main characteristics of the motion of a steel particle falling in fluid and colliding with the bottom of a vessel, including the particle velocity and the features of the collision, are captured well by our model, thus verifying its accuracy.

## IV. EFFECT OF RELATED PARAMETERS ON PARTICLE MOTION

According to Vojir and Michaelides,[16] the Basset force is important when a fine evaporating particle (the diameter about 1 $\mu$m) is driven by a sinusoidal flow velocity with the dimensionless frequency of fluid velocity fluctuations larger than 0.5. However, Vojir and Michaelides[16] also pointed out that the Basset force has little effect on the motion of particles with medium and large diameters, but the accurate range of the particle diameter is not defined by them. In our study, the diameter of the particle is 0.01 m that is significantly larger than the particle diameter 1 $\mu$m studied by Vojir and Michaelides.[16] In addition, it can be seen from Eq. (3) that the Basset force decreases with increasing Reynolds number and omitting the Basset force term can noticeably improve the calculation efficiency. Therefore, it is necessary to discuss the contribution of the Basset force to the particle velocities with various vibrational parameters of the riser.

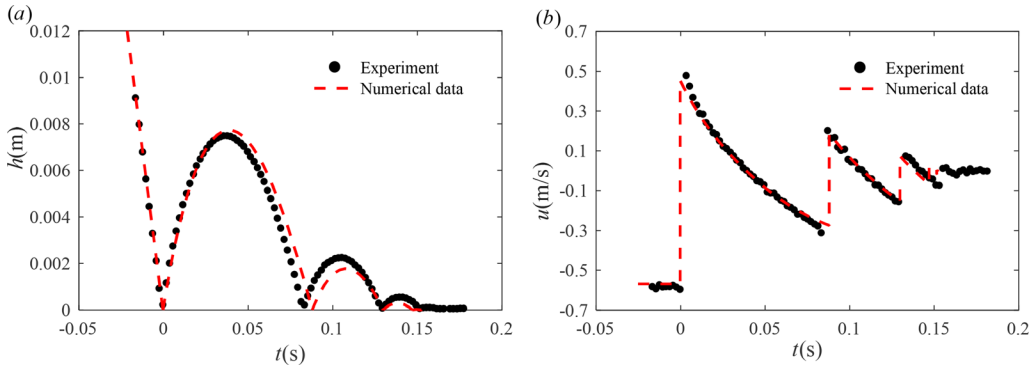


**FIG. 3.** Comparisons of (a) particle displacement and (b) particle velocity between experimental data and numerical results.

In this section, the motion of a sphere in a transverse vibration riser with upward Poiseuille flow is investigated first. The direction of riser vibration is taken as $x$ direction. The dimensionless velocity of the Poiseuille flow in the vertical riser can be expressed as

$$\mathbf{u}_f^* = \left[w^* A_m^* \cos\left(w^* t + \varphi_0\right)\right]\mathbf{i} + 0\mathbf{j} + \left[1 - \frac{\left(x_p^* - x_c^*\right)^2 + \left(y_p^* - y_c^*\right)^2}{R^{*2}}\right]\mathbf{k}, \tag{38}$$

where the dimensionless amplitude, angular frequency, and initial phase of the oscillation riser are denoted by $A_m$, $w$, and $\varphi_0$, respectively. In this section, the modulus of elasticity of the riser and particle, $E_w$ and $E_p$, are set as 200 and 60 GPa, respectively, the Poisson's ratios $\mu_w$ and $\mu_p$ are set as 0.3 and 0.26, the restitution coefficients in the normal and tangential directions are set as 0.76 and 0.7,[68] respectively, and the friction coefficient is set as 0.2.

The effect of the Basset force on the particle motion in a lateral vibration riser with Poiseuille flow is examined. In this examination, the diameter ratio $D/d = 10$, the vibration amplitude $A_m = 1.0$, and the frequencies $f = 0$, 0.05, and 0.2, where the case of $f = 0$ indicates that the riser is fixed and without any movement. In the case of $f = 0$, the particle is released from $x_p = 0.3$ and $y_p = 0.3$. The lateral and vertical velocities of the particle with and without Basset force for different vibrational frequencies are depicted in Fig. 4. It can be seen that the Basset force has no effect on the particle velocities regardless of collisions, indicating that the Basset force can be ignored during our study. Therefore, in order to improve calculation efficiency, the following investigation is conducted without considering the Basset force.

Owing to the absence of fluid shear in the validation of Sec. III, there is no Saffman force on the moving particle and therefore, the calculation is appropriate to test whether the Saffman force induced by the fluid shear force exerts any impact on the particle motion. Here, the particle is released from different initial distances away from the riser centerline to observe the particle motion in stationary riser with upward Poiseuille flow. Here, the diameter ratio is $D/d = 10$, and the vibration amplitude and frequency are set as 0.

The variation of the particle displacement and velocities with time are shown in Fig. 5. It can be seen from Fig. 5(a) that the particle moves rapidly to the centerline of the riser after being released, which is consistent with the experimental and theoretical results of Saffman[30] and Segre and Silberberg.[33] This can be attributed to the lateral velocity of the particle induced by the Saffman force. Furthermore, as the distance between the position at which the particle is released and the riser wall is decreased, the maximum lateral velocity of the particle becomes larger, which can be explained by the fact that the shear in the flow field is stronger near the wall than near the centerline of the riser. This is consistent with the properties of Poiseuille flow. It can also be observed from Figs. 5(b) and 5(c) that the lateral velocity $v_{px}$ and vertical velocity $v_{pz}$ increase rapidly and then decrease to a certain degree as the particle moves toward the axis of the riser, regardless of where it is initially released. That is, the position at which the particle is released has no effect on the terminal velocity of the particle under given conditions of Poiseuille flow and particle parameters. It should be noted that it is the effect of the Saffman force that is mainly under consideration here. Although no direct comparison with experimental data has been made here, the lateral displacement and the lateral and vertical velocities of a particle related to the Saffman force in Poiseuille flow do show similar trends to those found by Saffman[30] and by Segre and Silberberg,[33] which again proves the accuracy of our proposed model. Therefore, it is reasonable to use this model to investigate the particle motion in a vibrating riser.

In addition, the effects of the initial position of release of the particle, the oscillation amplitude, and the oscillation frequency of the riser on the particle motion are analyzed and discussed in Secs. IV A and IV B, respectively, as are those of collisions in Sec. IV C. Furthermore, the possible trajectories of the particle affected by the vibrational frequency and amplitude of the riser are summarized in Sec. IV D.

### A. Initial position of release of the particle in oscillation riser

Then, the effect of the initial position of release of the particle on the particle motion is studied. The dimensionless amplitude of the vibrating riser is set as $A_m = D = 1$, with two dimensionless frequencies $f = 0.05$ and 0.15 and an initial phase $\varphi_0 = 0$. The initial position of the

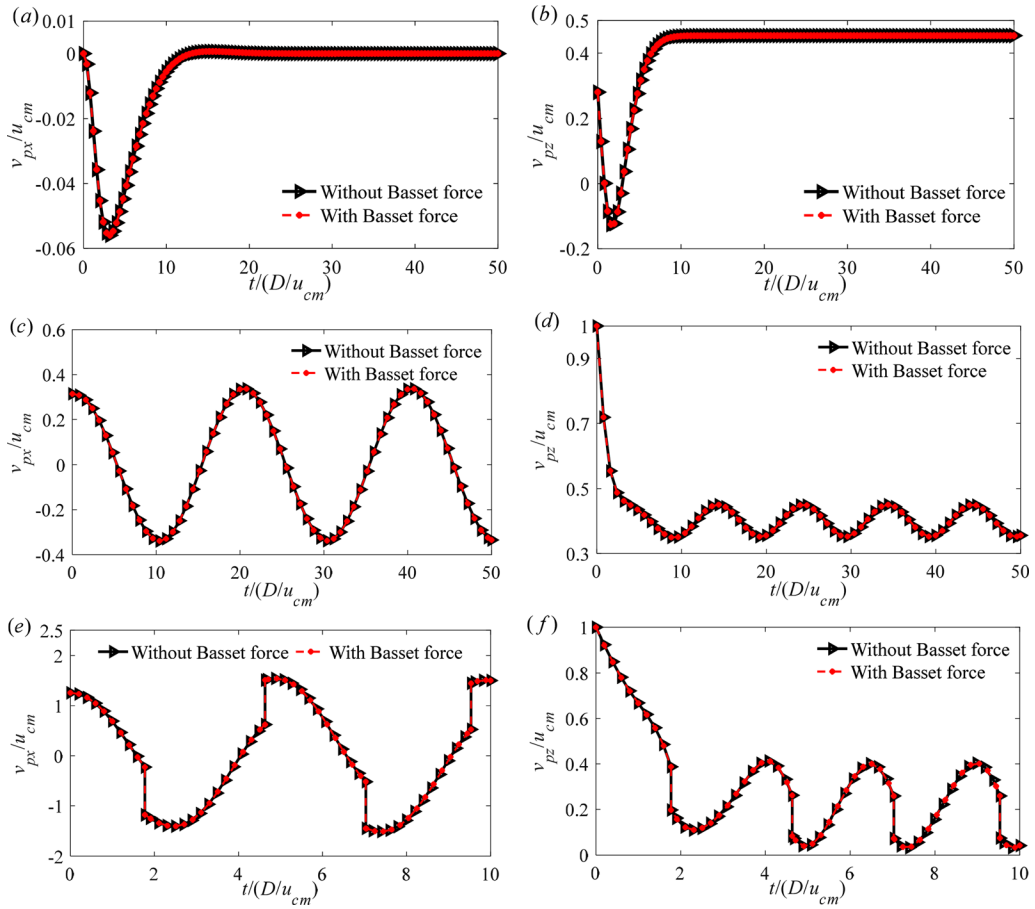


**FIG. 4.** Particle velocities with and without Basset force for different frequencies: lateral velocity in $x$ direction with (a) $f=0$, (c) $f=0.05$, and (e) $f=0.2$ and vertical velocity with (b) $f=0$, (d) $f=0.05$, and (f) $f=0.2$.

riser is given by $x_{c0} = A_m \sin\varphi_0, y_{c0} = 0$, while the initial position of the particle is given by $x_{p0} = y_{p0}, z_{p0} = 0$ and its initial velocity by $v_{px0} = wA_m \cos\varphi_0, v_{py0} = 0, v_{pz0} = 1 - [(x_{p0} - x_{c0})^2 + (y_{p0} - y_{c0})^2]/R^2$.

The corresponding particle displacements and velocities in the vibrating riser without and with collisions are shown in Figs. 6 and 7, respectively. It can be seen from Fig. 6 that the initial position of release of the particle has an effect on particle motion when the particle begins to move. However, the effect tends to be disappeared over time. Such evolution of the particle velocities and displacements can be explained based on the governing equations of particle motion in three directions ($x$, $y$, and $z$ directions), which are expressed as follows:

$$\frac{dv_{px}}{dt} = \lambda\left[\begin{array}{l}\frac{3}{4}C_D|\mathbf{u}_f - \mathbf{v}_p|(u_{fx} - v_{px}) + \frac{1}{2}\frac{du_{fx}}{dt} + \frac{Du_{fx}}{Dt} \\ \quad + \frac{3}{4}C_{LS}(\omega_{fz}u_{yre} - \omega_{fy}u_{zre}) \\ \quad + \frac{3}{12}C_H\sqrt{\frac{\pi}{Re_{cm}}}\int_0^t \frac{d(u_{fx} - v_{px})}{\sqrt{t-\tau}}d\tau\end{array}\right], \tag{39}$$

$$\frac{dv_{py}}{dt} = \lambda\left[\begin{array}{l}\frac{3}{4}C_D|\mathbf{u}_f - \mathbf{v}_p|(u_{fy} - v_{py}) + \frac{1}{2}\frac{du_{fy}}{dt} \\ \quad + \frac{Du_{fy}}{Dt} + \frac{3}{4}C_{LS}(\omega_{fx}u_{zre} - \omega_{fz}u_{xre}) \\ \quad + \frac{3}{12}C_H\sqrt{\frac{\pi}{Re_{cm}}}\int_0^t \frac{d(u_{fy} - v_{py})}{\sqrt{t-\tau}}d\tau\end{array}\right], \tag{40}$$

$$\frac{dv_{pz}}{dt} = \lambda\left[\begin{array}{l}\frac{3}{4}C_D|\mathbf{u}_f - \mathbf{v}_p|(u_{fz} - v_{pz}) \\ \quad + \frac{1}{2}\frac{du_{fz}}{dt} + \frac{Du_{fz}}{Dt} - (1-\beta)Fr \\ \quad + \frac{3}{4}C_{LS}(\omega_{fy}u_{xre} - \omega_{xz}u_{yre}) \\ \quad + \frac{3}{12}C_H\sqrt{\frac{\pi}{Re_{cm}}}\int_0^t \frac{d(u_{fz} - v_{pz})}{\sqrt{t-\tau}}d\tau\end{array}\right], \tag{41}$$

where the expression of fluid velocity $\boldsymbol{u}_f$ is shown in Eq. (38), and the fluid vorticity $\boldsymbol{\omega}_f$ is denoted as

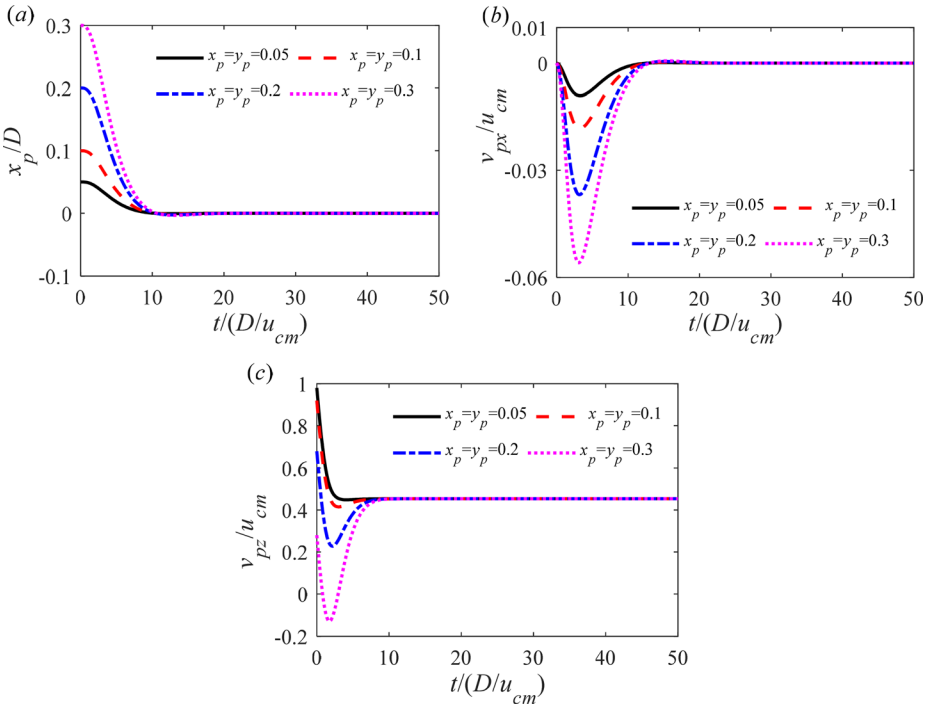


**FIG. 5.** (a) Lateral displacement, (b) lateral velocity, and (c) vertical velocity of particles with different initial positions of release.

$$\boldsymbol{\omega}_f = \frac{1}{2}\nabla \times \mathbf{u}_f = \frac{1}{2}\nabla \times \left\{ wA_m \cos(wt+\varphi_0)\mathbf{i} + 0\mathbf{j} + \left[1 - \frac{(x_p-x_c)^2 + (y_p-y_c)^2}{R^2}\right]\mathbf{k} \right\} = \frac{y_p-y_c}{R^2}\mathbf{i} + \frac{x_p-x_c}{R^2}\mathbf{j} + 0\mathbf{k} = \omega_{fx}\mathbf{i} + \omega_{fy}\mathbf{j} + \omega_{fz}\mathbf{k}. \tag{42}$$

The initial velocities of the particle are set as $(v_{px0}, v_{py0}, v_{pz0})$ mentioned at the beginning of Sec. IV A.

With the above-mentioned equations, it is indisputable that the terms of Saffman force and Basset force are nonlinear regardless of the velocity of the flow field. In our study, the fluid velocity inside the riser is assumed to a Poiseuille flow, and hence, the forces of drag, added mass, and stress-gradients are nonlinear in the $z$ direction due to the nonlinearity in the velocity profile of the flow fluid. Furthermore, the nonlinearity of the drag force in the other two directions ($x$ and $y$) is determined by drag coefficient $C_D$. When $Re_p$ is larger than 1, the drag force is nonlinear. While $Re_p \leq 1$, $C_D$ is equal to $\frac{24}{Re_p}$ K, and in $x$ and $y$ directions, the drag force can be expressed as a linear function $\frac{18\mu}{\rho_f d}(u_{fi} - v_{pi})$ of the relative velocity in those directions. Consequently, it is the presence of these non-linearities that presents significant challenges in obtaining the theoretical solution of the particle motion. So that, the characteristics of the particle motion can be explained by analyzing the calculation results and the flow field properties.

First, in the $y$ direction, the particle velocity is initially dominated by Saffman force at $t=0$, causing that it moves toward the riser axis. However, when $t>0$, a velocity difference arises, resulting in a non-zero drag force exerting on the particle, so the particle is subjected to the combined action of Saffman force and drag force. The former force acts toward the riser axis, while the latter opposes the direction of the relative velocity $\mathbf{v}_{pi} - \mathbf{u}_{fi}$. As shown in Fig. 6(d), during the early period following particle release, the particle velocity increases rapidly and reaches its maximum due to the fact that the Saffman force is greater than the drag force. Nevertheless, as the particle approaches the riser axis, the Saffman force decreases. After the moment when $v_{py}/u_{cm}$ reaches its peak, the Saffman force is less than the drag force, resulting in a reduction in $v_{py}/u_{cm}$. Upon reaching the riser axis [as depicted in Fig. 6(b)], the Saffman force vanishes, and concurrently, $v_{py}/u_{cm}$ diminishes to 0, leading to the absence of drag force and the cessation of particle motion in the $y$ direction. Additionally, the evolution of $v_{py}/u_{cm}$ always exists in this way regardless of whether a collision occurs between the particle and the riser wall.

As for the motion in the $x$ direction in which the riser undergoes vibrations, at $t=0$, apart from the Saffman force, the particle experiences the added mass force due to non-zero value of $\frac{d\mathbf{v}_{pi}}{dt} - \frac{d\mathbf{u}_{fi}}{dt}$. As time progresses ($t>0$), in addition to these two forces mentioned above, the drag force arises because the particle cannot synchronize with the vibrating riser. In the early period of particle release $t=0$–20, the equal velocity of the particle and the riser at $t=0$ results in a slight value of the velocity difference $v_{pxre}/u_{cm}$ in the $x$ direction, causing a small drag force. Therefore, the magnitudes of these three forces approach each other, leading to the occurrence of fluctuations in $v_{pxre}/u_{cm}$ under their combined influence. However, as time continues to advance $t>20$, the carrying of the fluid exerted on the particle progressively intensifies. Eventually, the particle motion in the $x$ direction is dominated by this fluid carrying, as evidenced by the periodical variations observed in $v_{pxre}/u_{cm}$ and $x_r/D$ when $t>20$ [as shown in Figs. 6(a) and 6(c)].

In addition, at $t=0$, the particle is subjected to gravity and buoyancy in the $z$ direction, while at $t>0$, the drag force, added mass force,

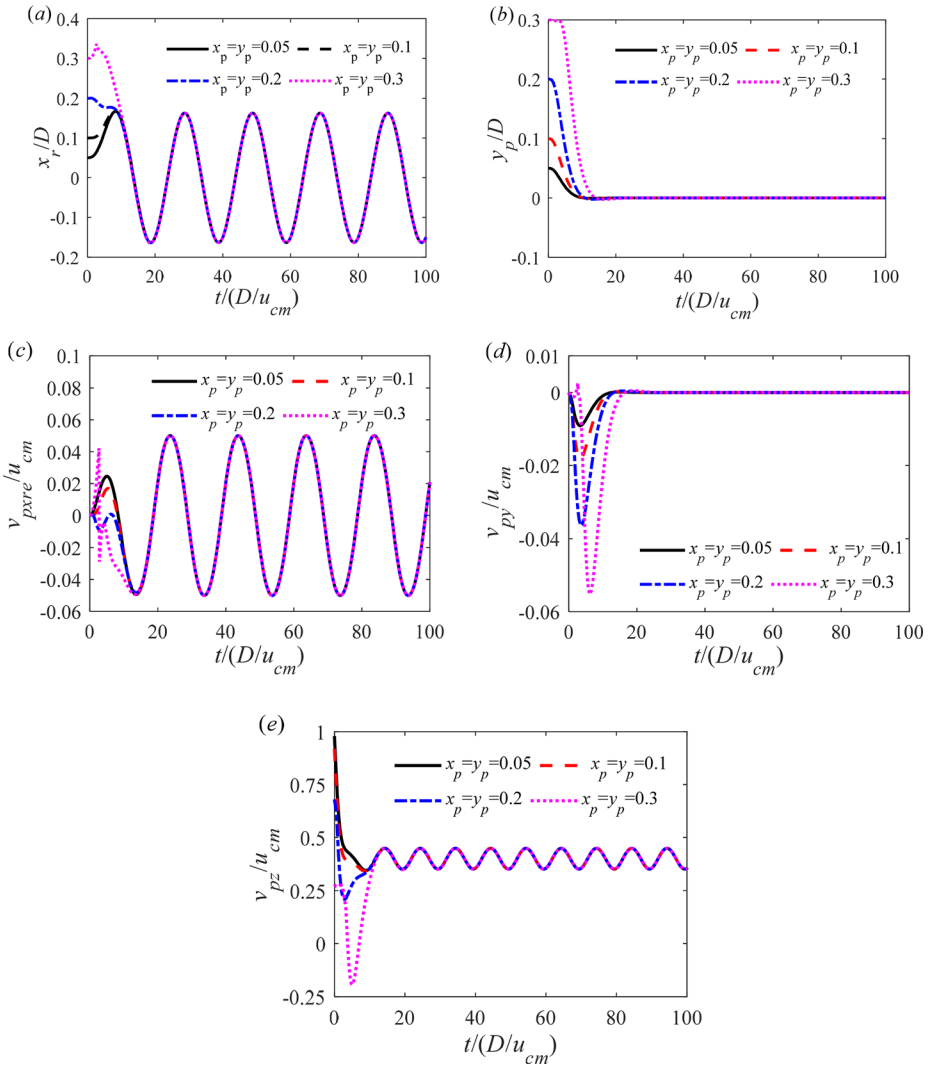


**FIG. 6.** Particle displacements and velocities for different initial positions of release of the particle without collisions ($f = 0.05$): (a) relative lateral displacement; (b) lateral displacement in $y$ direction; (c) relative lateral velocity in $x$ direction; (d) lateral velocity in $y$ direction; and (e) vertical velocity.

and Saffman force exert on the particle due to non-zero relative velocity between the particle and riser wall. During the initial period ($t = 0$–20), the vertical velocity of the particle is significantly influenced by its initial velocity and position due to the larger Saffman force near the riser wall and significant fluctuations in $v_{pxre}/u_{cm}$ and $x_r/D$. Note that the effect of the initial released position of the particle on $v_{pz}/u_{cm}$ diminishes over time. As shown in Figs. 6(a) and 7(a), the particle in the riser oscillates periodically around the riser centerline, resulting in a periodic variation of the vertical Poiseuille flow velocity acting on the particle. Consequently, in the vertical direction, forces (including drag force, added mass force, and Saffman force) with periodic changes exert on the particle. That is, the combined effect of the lateral motion of the particle and the characteristics of the Poiseuille flow field in the riser accounts for the regular oscillations of the particle's vertical velocity.

Additionally, as demonstrated in Fig. 7, the velocities and displacements of the particle are almost independent of the initial position. It can be explained by that compared to low vibrational frequencies (Fig. 6), increasing vibrational frequency enhances the carrying ability of the fluid on the particle, leading to an attenuation effect of the initial positions on the particle motion during the early period of particle release.

Therefore, it can be concluded that during the early period after particle release, the forces exerted on the particle arising from the ambient fluid are irregular and the particle motion is affected by the initial condition, owing to the combined action of several forces acting in opposition and their approaching magnitudes, or irregular acting on the sphere. However, once stable motion of the particle is achieved, the forces determined by the relative position, relative velocity, and velocity derivatives exhibit periodic variations, resulting in periodical oscillations of the particle velocity in $x$, $y$, and $z$ directions. Consequently, the initial released position of the particle has no effect on the stable particle movement in the transverse oscillation riser.

In addition, the magnitude of the velocity $v_{py}$ [Figs. 6(d) and 7(d)] is remarkably small compared with that of $v_{pxre}$ [Figs. 6(c) and 7(c)]. This can be explained by the dominant effect of riser vibration in

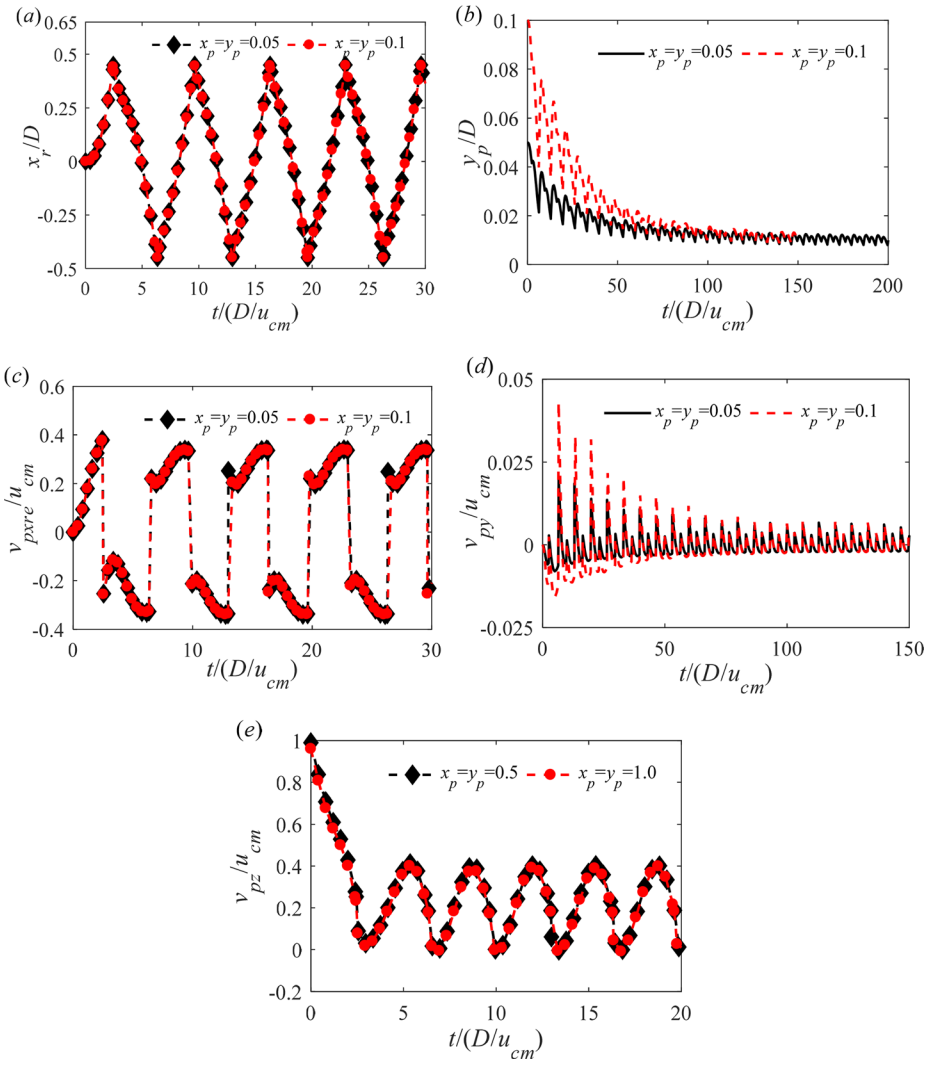


**FIG. 7.** Particle displacements and velocities for different initial positions of release of the particle with collisions ($f=0.15$): (a) relative lateral displacement; (b) lateral displacement in $y$ direction; (c) relative lateral velocity in $x$ direction; (d) lateral velocity in $y$ direction; and (e) vertical velocity.

the $x$ direction. When the particle moves in the transversely vibrating riser with Poiseuille flow, the motion of the particle in the direction corresponding to the riser oscillation (the $x$ direction) is determined by both riser vibration and the Saffman force, while its motion perpendicular to the riser vibration (the $y$ direction) is mainly induced by the Saffman force rather than the riser oscillation. Although the particle motion can be influenced by the Saffman force, the induced velocities in two directions are notably small, as can be seen from the velocity $v_{py}$ in Figs. 6(d) and 7(d). From Figs. 6(b) and 7(b), it can also be seen that the particle displacement $y_p$ in the $y$ direction eventually tends to zero, meaning that the motion of the particle is scarcely affected by its velocity and displacement in the $y$ direction, regardless of its initial position of release. Since the characteristics of particle motion in the $y$ direction are hardly impacted by the riser vibration in the $x$ direction, it is mainly the particle velocity and displacement in the lateral $x$ direction and vertical $z$ direction that will be analyzed in Subsections IV B–IV D.

## B. Riser vibration

It has been shown above that the particle velocity and displacement in the $y$ direction can generally be neglected compared with those in the lateral $x$ direction and vertical $z$ direction. Therefore, the effects of variations in the amplitude and frequency of the riser vibrations on the characteristics of particle motion in the lateral $x$ direction and vertical $z$ direction will be investigated here.

### 1. Vibrational frequency

Here, the amplitude of riser vibration is fixed as $A_m=D=1$, while its oscillation frequency is varied as $f=0.025$, 0.05, 0.1, 0.2, 0.3, and 0.4. The internal Poiseuille flow is again expressed as in Eq. (29). The corresponding time histories of the relative lateral velocity are presented in Fig. 8. Note that to demonstrate the results more clearly, the time histories here and in Figs. 9 and 10 are nondimensionalized by the vibrational period $T$ of the riser.

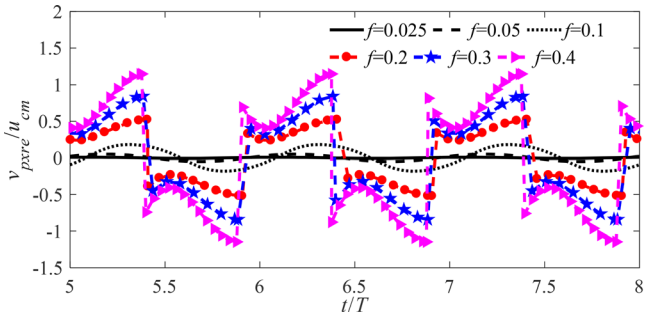


**FIG. 8.** Relative lateral velocity for different vibrational frequencies of the riser.

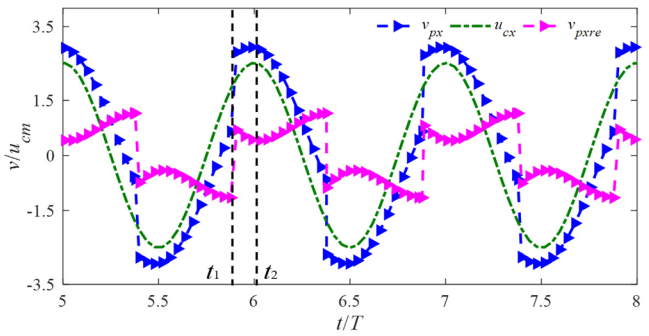


**FIG. 9.** Lateral velocities of the particle and the riser at $f = 0.4$.

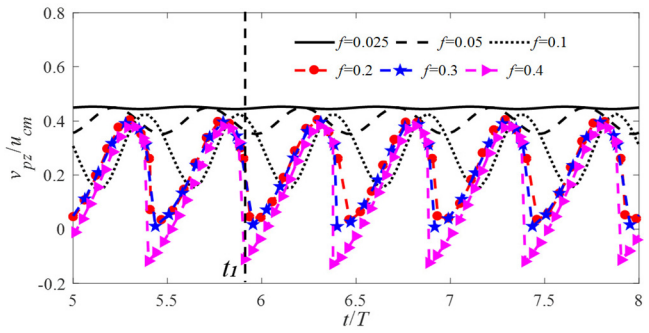


**FIG. 10.** Vertical velocity of the particle for different vibrational frequencies of the riser.

It can be seen from Fig. 8 that a higher vibrational frequency of the riser leads to larger magnitudes of the lateral velocity $v_{pxre}$ of the particle relative to the riser, which means that the ability of the particle to catch up with the oscillating riser is weakened at high vibrational frequencies. For example, the maximum value of the relative lateral velocity is equal to 0.049 at $f = 0.05$. When the riser's vibrational frequency is increased to 0.4, the maximum value of the relative lateral velocity is increased to 1.149. Furthermore, regardless of collisions between the particle and the riser, the relative lateral velocity always changes periodically. In the absence of collisions, the relative lateral velocity $v_{pxre}$ varies smoothly with time, whereas a collision between the particle and the riser will lead to a jump in $v_{pxre}$, as can be observed in Fig. 9. When a collision occurs, there is a reversal in the relative lateral velocity due to the sudden change in particle motion, and at the time of collision, $v_{pxre}$ attains a large magnitude. As can be seen in Fig. 9, a collision occurs at $t/T = t_1$, resulting in a jump in the lateral velocity $v_{px}$ of the particle as well as a reversal in the relative lateral velocity $v_{pxre}$ between the particle and the vibrating riser with $f = 0.4$. As time proceeds further, $v_{px}$ approaches its maximum, while $v_{pxre}$ decreases slightly to a minimum at $t/T = t_2$. This decrease in $v_{pxre}$ can be attributed to the weakening influence of the collision. As both the particle and riser continue to move, the internal flow again comes have the dominant effect on particle motion, concurrent with the decaying effect of the collision. Consequently, the magnitude of the relative lateral velocity increases gradually after its minimum at $t/T = t_2$, and it continues to increase until the next collision occurs between the particle and the vibrating riser.

The behavior of the vertical velocity of the particle is depicted in Fig. 10. It can be seen that the vertical particle velocity varies periodically with a frequency approximately twice that of the riser. This can be explained by the symmetries of the Poiseuille flow field and the particle displacement around the riser axis (as shown in Fig. 12). The particle moves in the transversely vibrating riser with Poiseuille flow $1 - \frac{(x_p - x_c)^2 + (y_p - y_c)^2}{R^2}$, which exhibits symmetry about the riser axis $(x_c, y_c)$ in terms of vertical velocity. Furthermore, as depicted in Fig. 12, a periodical variation of the relative displacement between the particle and riser axis can be found. The values of peaks and valleys within one period are equal, indicating that the particle moves symmetrically around the riser axis. Under the combination effect of fluid and riser vibration, the particle travels through the flow field with symmetrical vertical velocity two times within one vibrational period; as a result, the vertical particle velocity presents periodic variation with a frequency approximately twice as that of the riser frequency.

Additionally, it is also clear that collisions between the particle and the vibrating riser have an effect in reducing the vertical velocity of the particle. As can be seen from Fig. 10, when $f = 0.3$, before the collision at $t/T = t_1$, the particle has a vertical velocity $v_{pz}/u_{cm} = 0.3119$, whereas after the collision, this decreases to $v_{pz}/u_{cm} = 0.0105$. The reason for the decrease in particle vertical velocity after collision will be introduced in combination with the reason for the decrease in the lifting distance of the particle with increasing vibrational frequency.

Since the lifting distance of the particle plays a vital role in determining the lifting efficiency of the riser, it is important to consider how this lifting distance changes under different vibrational frequencies of the riser. Here, the lifting distance of the particle is calculated over the same time interval for different values of the vibrational frequency. As can be seen from Fig. 11, the lifting distance of the particle decreases with increasing vibrational frequency, indicating that the efficiency of ore haulage is influenced by the vibrational frequency of the riser. At higher vibrational frequencies, the efficiency of ore haulage is reduced. This variation in the lifting distance of the particle can be ascribed to the variations in lateral particle motion. In the absence of collisions, it can be seen from Fig. 12(a) that as the vibrational frequency of the riser is increased, the amplitude of the lateral displacement of the particle relative to the riser centerline is increased. Consequently, the particle moves closer to the riser wall, and the vertical fluid flow velocity that it experiences is reduced. This leads to a decrease in the vertical particle velocity, and so the particle is conveyed

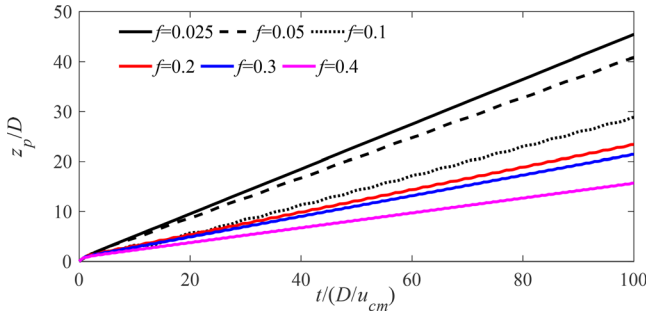


**FIG. 11.** Lifting distance of particle for different vibrational frequencies of the riser.

more slowly, resulting in its lifting distance in the vibrating riser being reduced. More importantly, however, it can be seen from Fig. 12(b) that when collisions do occur, the amplitudes of the relative lateral displacement under different riser vibrational frequencies are the same, indicating that the variations in the particle lifting distance are scarcely affected by the internal flow in this situation. That is, the reduction of the lifting distance of the particle is dominated by collisions, which demonstrates the crucial effect of collisions on the lifting efficiency of the riser.

In the case considered in this study, when a collision occurs between the particle and the riser, the condition $k_\tau|\delta_\tau| > \mu_f|k_n\delta_n|$ is satisfied throughout the collision process. The tangential force can, then, be calculated as $\mathbf{F}_{\tau z} = -\mu_f|k_n\delta_n|\delta_{\tau z}/|\delta_{\tau z}|\boldsymbol{\tau}_z$. It can be seen that $\mathbf{F}_{\tau z}$ is related to the normal parameters $k_n$ and $\delta_n$ and the friction coefficient $\mu_f$, which depends on the particle and riser materials. The results

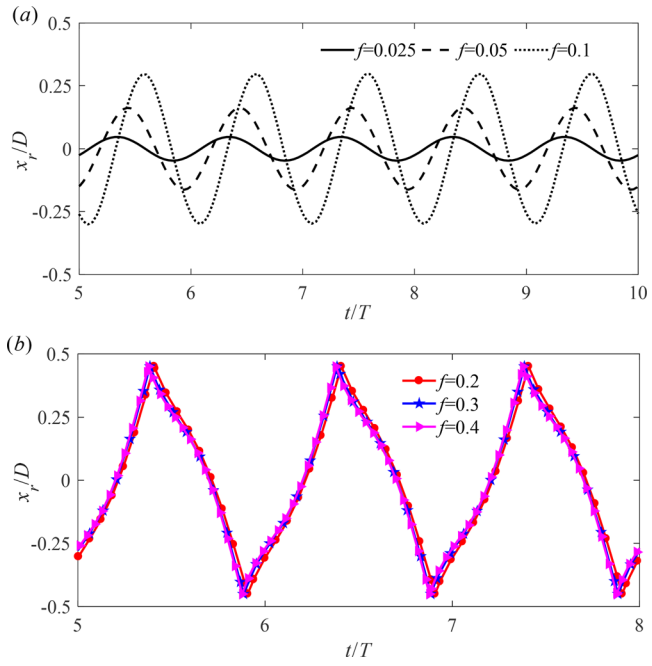


**FIG. 12.** Relative lateral displacement of the particle for different vibrational frequencies of the riser: (a) without collisions and (b) with collisions.

in Fig. 8 have shown that the relative lateral velocity can be increased by increasing the vibrational frequency of the riser. As this frequency increases, the maximum normal overlap exhibits an increasing trend, as shown in Fig. 13(a). From the values of $\delta_n$ [Fig. 13(a)] and $\delta_{\tau z}$ [Fig. 13(b)], the particle acceleration can be obtained. The relative vertical velocity of the particle can then be calculated, as shown in Fig. 13(c), from which it can be seen that at higher vibrational frequencies of the riser, the relative vertical velocity of the particle tends to become small after a collision. As a consequence, the lifting distance of the particle decreases with increasing vibrational frequency when collisions do occur.

#### 2. Vibrational amplitude

In addition to the vibrational frequency of the riser, changes in its vibrational amplitude can also exert an impact on the motion of the particle. Therefore, the motion of the particle in upward Poiseuille flow is investigated for five vibrational amplitudes $A_m = 0.5$, 0.75, 1, 1.5, and 2.0 and two vibrational frequencies $f = 0.05$ and 0.3. The aim of choosing two vibrational frequencies here is to ensure that collisions occur between the particle and the vibrating riser. The variations in the velocities and the lifting distance of the particle are displayed in Figs. 14–16.

It is clear from Figs. 14(a) and 15(a) that an increase in the vibrational amplitude of the riser will increase the relative lateral velocity $v_{pxre}$ of the particle regardless of collisions. When $f = 0.05$, $v_{pxre} = 0.0214$ at $A_m = 0.5$. When the vibrational amplitude of the riser is increased to 2.0, the relative lateral velocity reaches 0.14. This phenomenon can be explained by the fact that with increasing vibrational amplitude of the riser, the relative motion between the particle and oscillation riser is intensified, resulting in an increase in the relative lateral velocity between them, whether or not collisions occur.

Furthermore, as shown in Fig. 14(b), at a riser vibrational frequency $f = 0.05$, the vertical velocity $v_{pz}$ of the particle decreases significantly with increasing riser vibrational amplitude, which implies that the lifting distance of the particle will also decrease when the vibrational amplitude is increased. Collisions do not occur at the low vibrational frequency of $f = 0.05$, and so the vertical velocity of the particle is mainly affected by the internal flow, as pointed out in Sec. IV B 1. At a higher vibrational frequency of $f = 0.3$, for which collisions between the particle and the riser do occur, it can be seen from Fig. 15(b) that $v_{pz}$ decreases slightly with increasing vibrational amplitude of the riser. It is evident that at a high vibrational frequency, collisions have a dominant effect on the relatively lateral velocity and vertical velocity of the particle. From Fig. 16, it can also be seen that the lifting distance of the particle decreases with increasing vibrational amplitude of the riser, regardless of collisions and the vibrational frequency. This behavior can again be attributed to the effects of both internal flow and collisions, as described in Sec. IV B 1.

### C. Collisions between particle and vibrating riser

It has been shown above that collisions between the particle and vibrating riser will occur at high vibrational frequencies and amplitudes of the riser, and it is, therefore, necessary to explore the effects of these collisions on the motion of the particle. The time histories of the riser vibrational displacement $x_p$, the displacement of the particle relative to the riser centerline $x_r$, the lateral velocity $v_{px}$, and the vertical

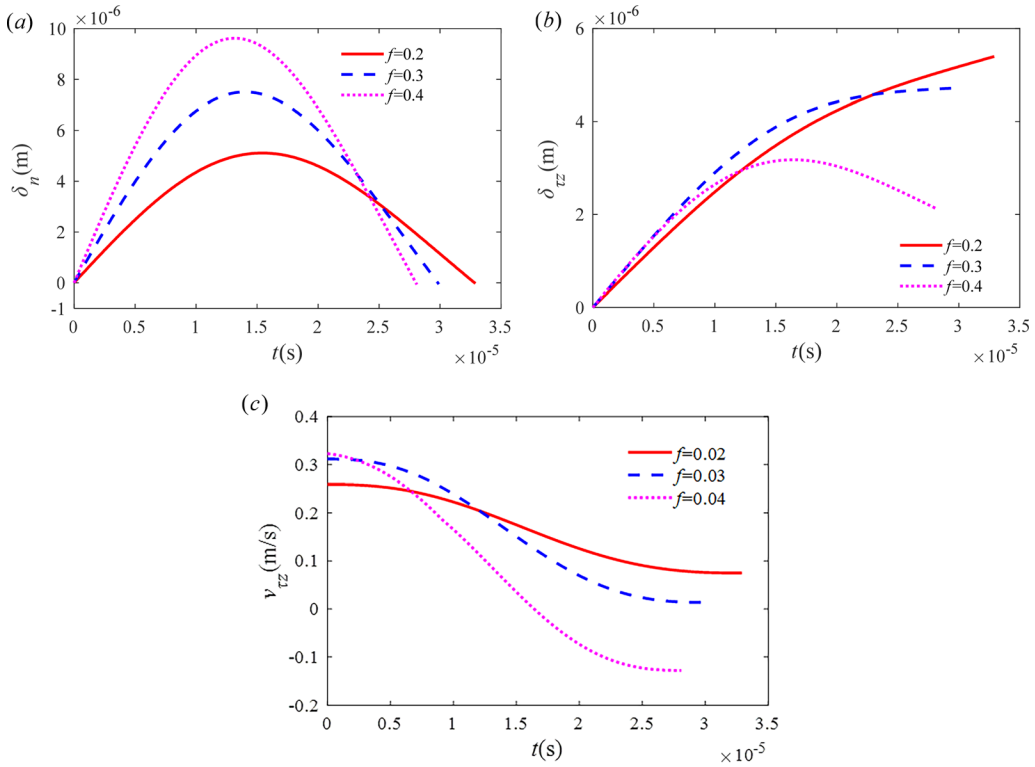


**FIG. 13.** Variations of (a) normal overlap, (b) tangential overlap, and (c) relative vertical velocity of the particle during a collision.

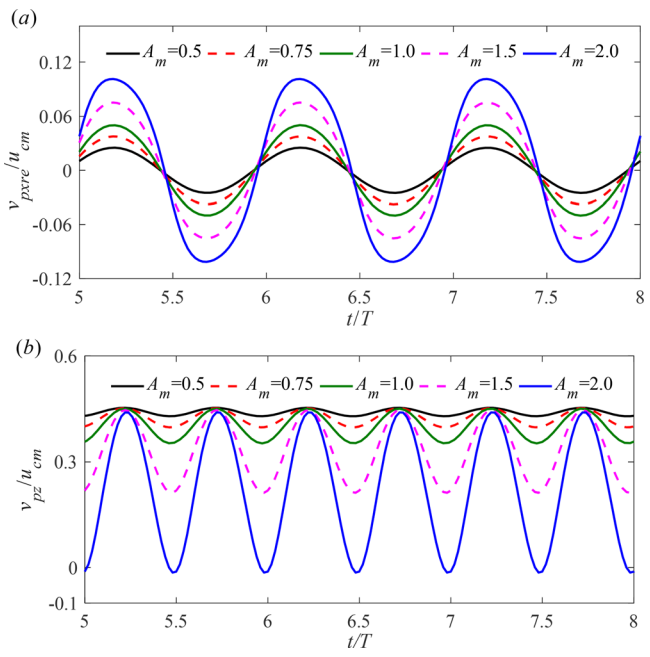


**FIG. 14.** (a) Relative lateral velocity and (b) vertical velocity of the particle for different vibrational amplitudes of the riser without collisions ($f = 0.05$).

velocity $v_{pz}$ are shown in Figs. 17 and 18 for cases without collisions ($f = 0.05$) and with collisions ($f = 0.3$), respectively. In the plots of $x_p$, the upper and lower blue lines represent the time histories of the two riser walls in the direction of vibration.

It can be seen from Fig. 17 that when there are no collisions between the particle and the riser, the particle moves with the vibrating riser, with a relative displacement of less than the radius $R$ of the riser. The particle motion in the lateral direction cannot catch up with the riser vibrations, leading to a slight phase difference between the particle motion and the riser oscillations. The maximum relative displacement between the particle and the riser centerline coincides approximately with the moment at which the oscillating riser is at its equilibrium position (as shown by the red dots in Fig. 17).

In the presence of collisions, the particle motion still has to catch up with the riser vibrations, as can be seen from Fig. 18. In this case, however, the particle behavior is more complicated, and the displacement of the particle relative to the riser centerline and the lateral and vertical velocities are obviously affected by the collisions. As shown by the red dots in Fig. 18, the maximum relative displacement between the particle and the riser centerline coincides approximately with the moment at which the oscillating riser is at its maximum amplitude. This difference from the case without collisions ($f = 0.05$) indicates that the collisions between the particle and the vibrating riser have an effect on the phase difference of displacement. Collisions between the particle and the vibrating riser occur when the relative displacement reaches its maximum value, and $x_r$ begins to decrease immediately

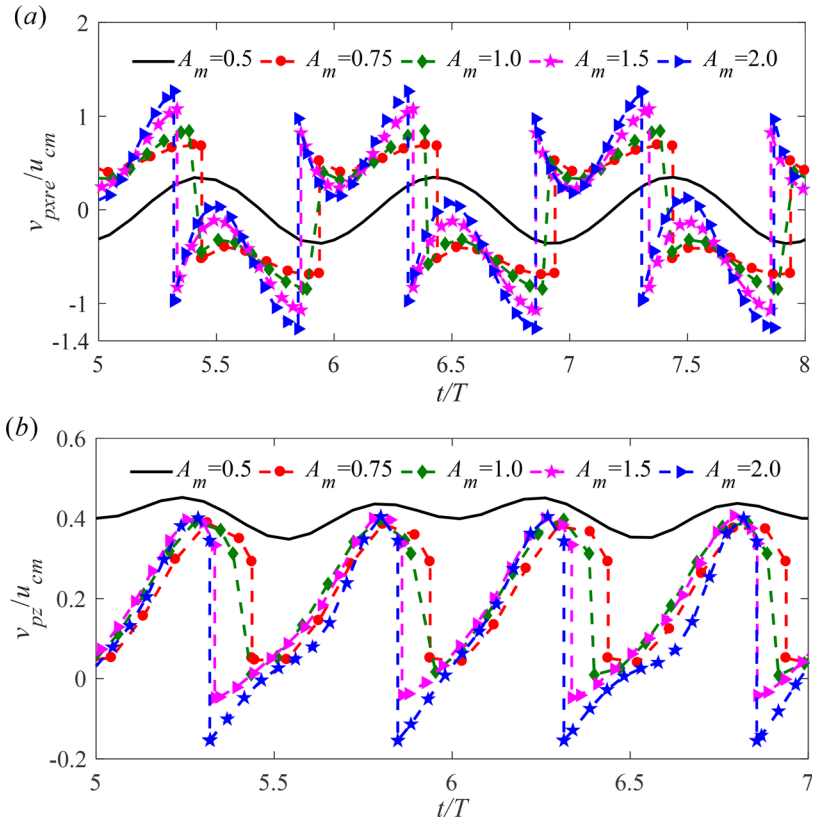


**FIG. 15.** (a) Relative lateral velocity and (b) vertical velocity of the particle for different vibrational amplitudes of the riser with collisions ($f = 0.3$).

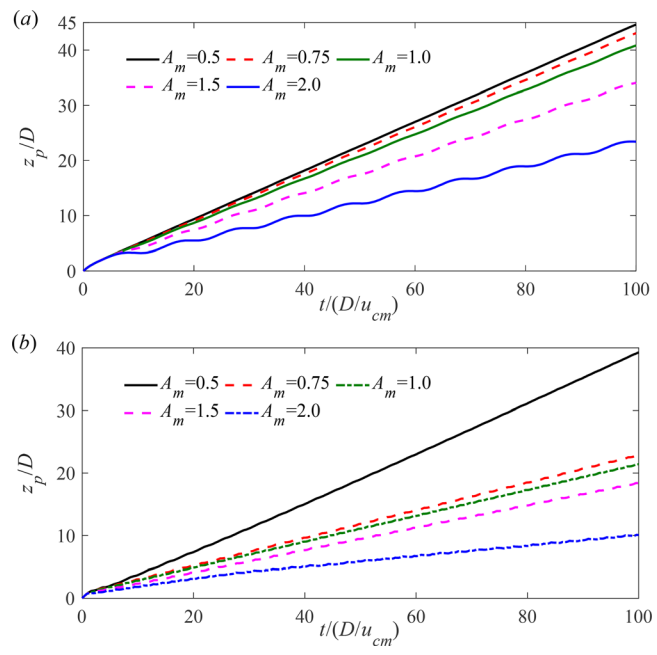


**FIG. 16.** Lifting distance of the particle for different vibrational amplitudes of the riser: (a) without collisions ($f = 0.05$) and (b) with collisions ($f = 0.3$).

after a collision. In addition, the lateral velocity and vertical velocity of the particle both exhibit a jump phenomenon due to collisions. The maximum value of the vertical velocity $v_{pz}$ coincides with the minimum value of the lateral velocity (as represented by the magenta dots

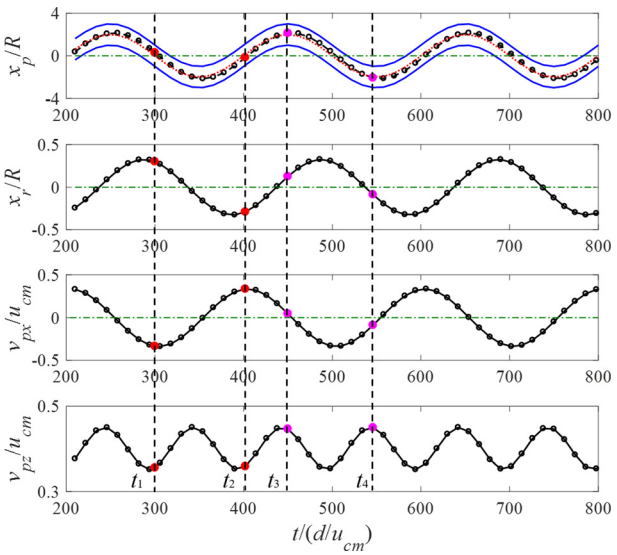


**FIG. 17.** Particle velocity and displacement without collisions ($f = 0.05$).

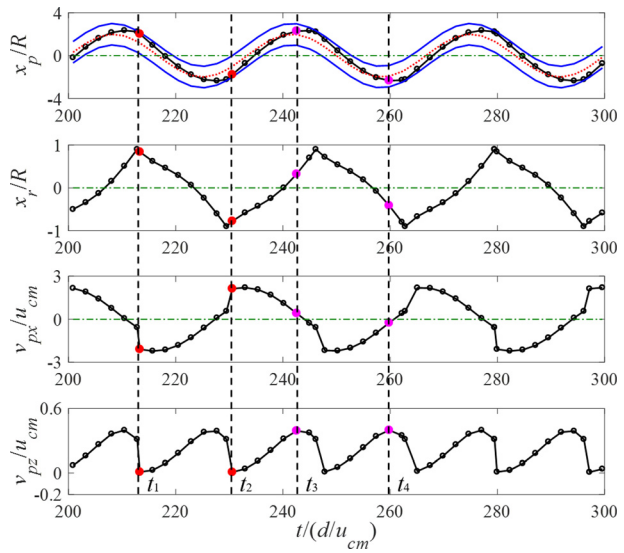


**FIG. 18.** Particle velocity and displacement with collisions ($f = 0.3$).

in Figs. 17 and 18), which can be explained by energy conservation in the two directions. As shown above, the lifting distance of the particle is related to both its lateral and vertical velocities, and therefore, collisions between the particle and the vibrating riser will affect the lifting distance through their effects on these two velocities.

Another important characteristic affected by collisions between the particle and the vibrating riser is the particle trajectory. Figure 19 shows the particle trajectories for vibrational frequencies $f = 0.05$ (in which case there are no collisions) and $f = 0.3$ (for which collisions do occur). It can be seen from Fig. 19(a) that in the absence of collisions, the particle moves along the riser centerline from bottom to top, following a smooth S-shaped trajectory. From Fig. 19(b), it is clear that the particle trajectory is influenced by collisions, which cause abrupt changes to the direction of particle motion.

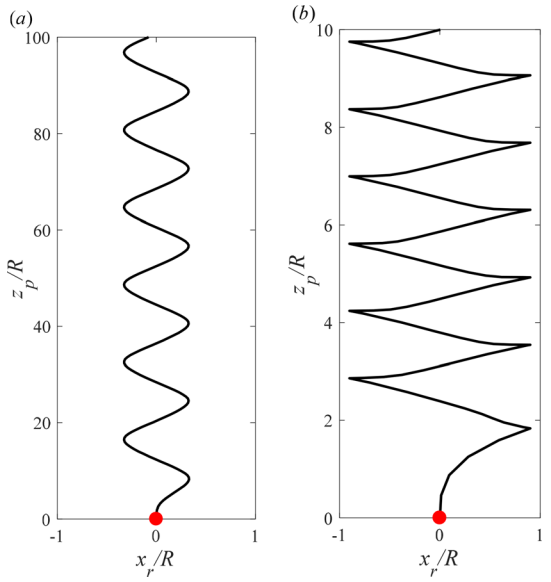


**FIG. 19.** Particle trajectories: (a) without collisions ($f = 0.05$) and (b) with collisions ($f = 0.3$).

### D. The regime map of the particle behaviors related to the riser vibration

In Secs. IV A–IV C, the particle motion with various vibrational frequencies and amplitudes is discussed. It is clear that the vibrational parameters ($A_m$, $f$) play an important role in the transformation of the particle movement regimes. Therefore, a regime map of the particle related to the vibrational frequency and amplitude of the riser is attempted to be established here. As this study aims at investigating the motion of particles for deep-sea mining, the parameters of the particle are set in reference to the density and diameter of ores. Correspondingly, the regime of the particle motion with $d = 0.01$ m and $\rho_f = 2000$ kg/m$^3$ is displayed in Fig. 20, wherein the domain is separated into three parts by two roughly line related to $A_m$ and $f$. It can be observed that the collision between the particle and the riser wall does not occur, which corresponds to the "*" region, as demonstrated in Figs. 20 and 21(a). Then, the collision between the particle and the riser wall appears once in the first period of the riser vibration in Fig. 21(b), which matches the red line with "★" in Fig. 20, indicating that the particle touches one side of the riser wall. The expression for this red line with "★" in Fig. 20 is $f \times (A_m - 0.0146) = 0.9627$, where $f$ and $A_m$ represent the dimensionless frequency and amplitude of the vibrating riser. As displayed in Figs. 21(c) and 21(d), the occurrence of collision can be detected over the first several periods of the riser vibration, after which the collision can be scarcely observed, which corresponds to the "+" region in Fig. 20. It is also presented in Fig. 21(e) that the collision can be captured twice in one vibrational period of the riser on the black line with "●" and in the "□" region, which means that the particle is in contact with both sides of the riser wall in one vibrational period. The expression for the black line with

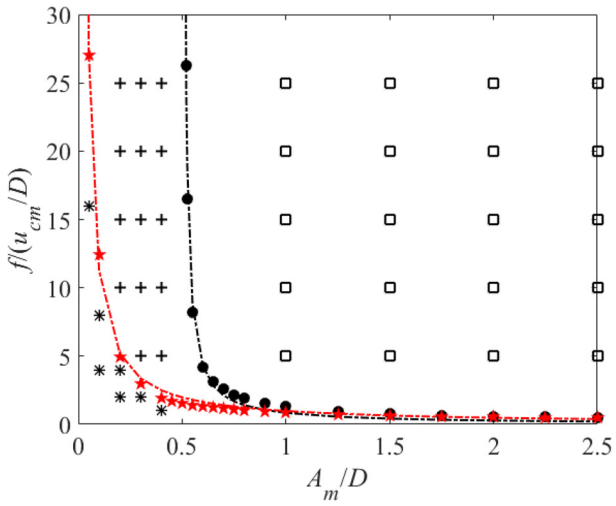


**FIG. 20.** The regime map of a particle trajectory with various vibrational frequencies and amplitudes of the riser.

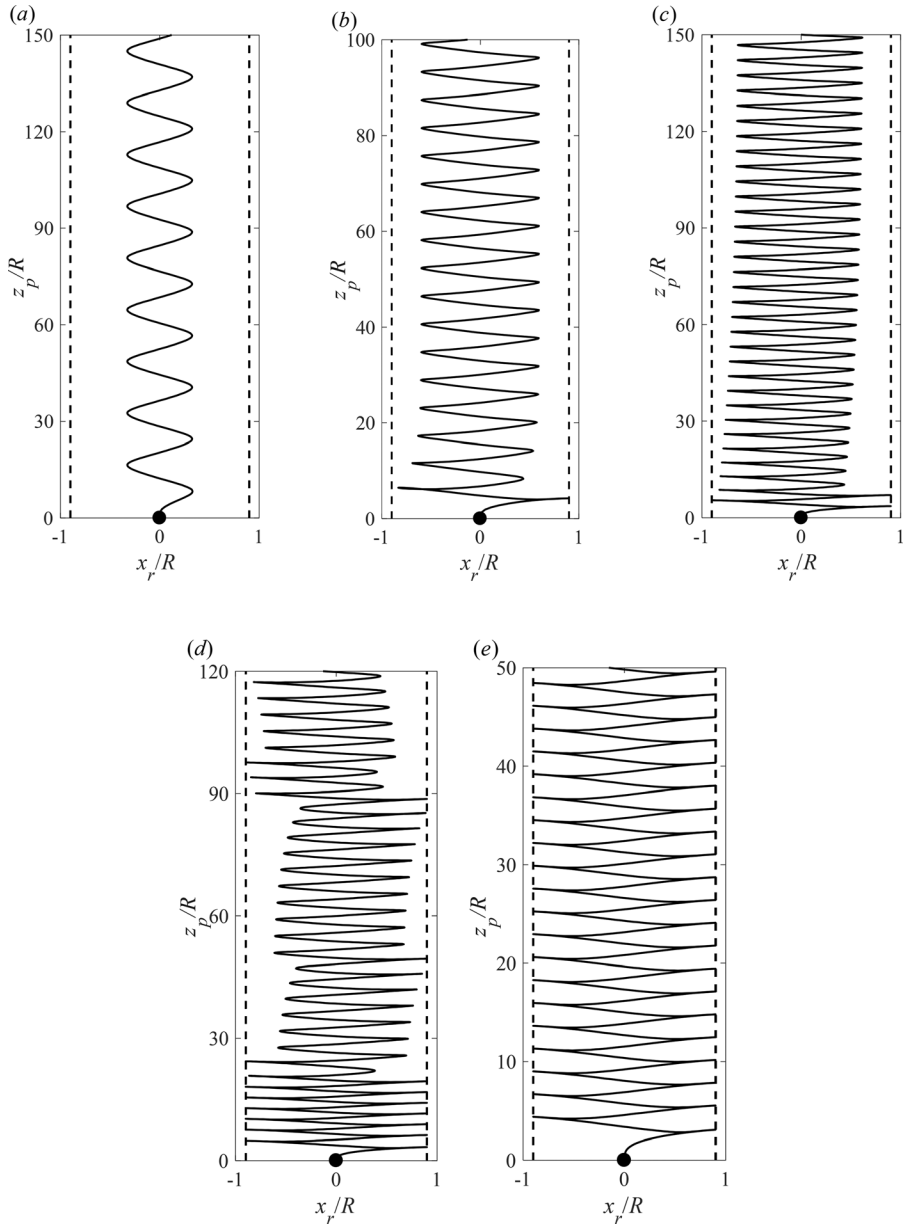


**FIG. 21.** The particle trajectory with various vibrational parameters: (a) $f = 0.05$ without collision; (b) $f = 0.0867$ collision occurs once; (c) $f = 0.1$ collisions occur over the first several periods; (d) $f = 0.12$ collisions occur over the first several periods and once after several periods; and (e) $f = 0.15$ collision occurs twice in one vibration period.

"●" in Fig. 20 is $f \times (A_m - 0.507) = 0.4168$, indicating that the twice collisions of the particle in one vibrational period of the riser cannot be observed when the vibration amplitude of the riser is less than the riser radius.

## V. CONCLUDING REMARKS

In this study, the motion of an ore in a lifting riser subjected to lateral vibrations has been investigated by using the governing equation for the motion of a spherical particle in Poiseuille flow and the Hertz–Mindlin soft sphere collision model. The particle velocities, displacement, and trajectory have been analyzed and discussed for various initial positions of release of the particle and various vibrational frequencies and amplitudes of the riser. The influence of collisions between the particle and the vibrating riser on the motion of the particle has also been investigated. Furthermore, a regime map of the particle related to the vibrational frequency and amplitude of the riser is established preliminarily. The results are likely to provide potential guidance on transporting the ores in lifting risers efficiently. The main conclusions that can be drawn from this study are as follows.

The initial position of release of the particle has no impact on the terminal characteristics of the particle motion. With increasing frequency and amplitude of the riser vibration, the relative lateral velocity of the particle increases owing to the intensified relative motion between the particle and riser, while the vertical velocity of the particle

decreases. The vertical velocity of the particle changes periodically with a frequency twice as the vibrational frequency of the riser. Increases in the vibrational frequency and amplitude of the riser both lead to a decrease in the lifting distance of the particle, which can be attributed to the effect of relative lateral velocity and the internal fluid field, as well as to collisions between the particle and the vibrating riser.

Collisions between the particle and the vibrating riser affect the particle motion, leading to a jump in the particle velocities, a phase difference between the displacements of the particle and the riser, and variations in the particle trajectory. With the various frequencies and amplitudes of the vibration riser, different regimes of the particle behavior in lateral vibration riser with upward Poiseuille flow can be observed.

It should be recognized that the present study is focused on the particle motion in a vibrating riser, and that further work is required to provide a more comprehensive understanding of the characteristics and underlying mechanisms of such particle motion in the context of developments in deep-sea mining technology, including the influence of particle count, particle gradation, and so on.

## ACKNOWLEDGMENTS

This work was supported by the National Natural Science Foundation of China (Grant Nos. 12132018, 12202455, and 11972352) and the Strategic Priority Research Program of the Chinese Academy of Sciences (Grant No. XDA22040304).

## AUTHOR DECLARATIONS

### Conflict of Interest

The authors have no conflicts to disclose.

### Author Contributions

**Mingzhu Wei:** Data curation (lead); Investigation (lead); Methodology (equal); Software (lead); Validation (lead); Visualization (equal); Writing – original draft (lead); Writing – review & editing (equal). **Jinlong Duan:** Investigation (equal); Resources (equal); Supervision (equal); Writing – review & editing (equal). **Xu Wang:** Funding acquisition (equal); Resources (equal); Supervision (equal); Writing – review & editing (equal). **Jifu Zhou:** Conceptualization (lead); Data curation (equal); Formal analysis (equal); Funding acquisition (equal); Investigation (equal); Methodology (lead); Project administration (equal); Resources (equal); Supervision (lead); Writing – review & editing (equal).

## DATA AVAILABILITY

The data that support the findings of this study are available from the corresponding author upon reasonable request.

## REFERENCES

[1]E. Romenski, D. Drikakis, and E. Toro, "Conservative models and numerical methods for compressible two-phase flow," J. Sci. Comput. **42**(1), 68–95 (2010).
[2]S. Busto, M. Dumbser, S. Gavrilyuk, and K. Ivanova, "On thermodynamically compatible finite volume methods and path-conservative ADER discontinuous Galerkin schemes for turbulent shallow water flows," J. Sci. Comput. **88**(1), 28 (2021).
[3]F. Thein, E. Romenski, and M. Dumbser, "Exact and numerical solutions of the Riemann problem for a conservative model of compressible two-phase flows," J. Sci. Comput. **93**(3), 83 (2022).
[4]E. Romenski, G. Reshetova, and I. Peshkov, "Two-phase hyperbolic model for porous media saturated with a viscous fluid and its application to wavefields simulation," Appl. Math. Modell. **106**, 567–600 (2022).
[5]B. Fu, L. Zou, and D. Wan, "Numerical study of vortex-induced vibrations of a flexible cylinder in an oscillatory flow," J. Fluids Struct. **77**, 170–181 (2018).
[6]Y. Qu and A. V. Metrikine, "A wake oscillator model with nonlinear coupling for the vortex-induced vibration of a rigid cylinder constrained to vibrate in the cross-flow direction," J. Sound Vib. **469**, 115161 (2020).
[7]J. Duan, J. Zhou, X. Wang, Y. You, and X. Bai, "Cross-flow vortex-induced vibration of a flexible fluid-conveying riser undergoing external oscillatory flow," Ocean Eng. **250**, 111030 (2022).
[8]C. Y. Li, Z. Chen, X. Lin, A. U. Weerasuriya, X. Zhang, Y. Fu, and T. K. T. Tse, "The linear-time-invariance notion to the Koopman analysis: The architecture, pedagogical rendering, and fluid–structure association," Phys. Fluids **34**(12), 125136 (2022).
[9]C. Y. Li, Z. Chen, T. K. T. Tse, A. U. Weerasuriya, X. Zhang, Y. Fu, and X. Lin, "The linear-time-invariance notion of the Koopman analysis. Part 2. Dynamic Koopman modes, physics interpretations and phenomenological analysis of the prism wake," J. Fluid Mech. **959**, A15 (2023).
[10]G. Magnus, "Ueber die abweichung der geschosse, und: Ueber eine auffallende erscheinung bei rotirenden körpern," Ann. Phys. **164**, 1 (1853).
[11]R. D. Mehta, "Aerodynamics of sports balls," Annu. Rev. Fluid Mech. **17**, 151–189 (1985).
[12]A. B. Basset, *A Treatise on Hydrodynamics* (Deighton, Bell and Co., Cambridge, 1888), Vol. 2, p. 21 (Also Dover Publications, Inc., New York, 1961).
[13]F. Odar and W. S. Hamilton, "Forces on a sphere accelerating in a viscous fluid," J. Fluid Mech. **18**, 302–314 (1964).
[14]E. E. Michaelides, "A novel way of computing the Basset term in unsteady multiphase flow computations," Phys. Fluids A **4**, 1579–1582 (1992).
[15]L. Liang and E. E. Michaelides, "The magnitude of Basset forces in unsteady multiphase flow computations," J. Fluids Eng. **114**, 417–419 (1992).
[16]D. J. Vojir and E. E. Michaelides, "Effect of the history term on the motion of rigid spheres in a viscous fluid," Int. J. Multiphase Flow **20**, 547–556 (1994).
[17]C. M. Tchen, "Mean value and correlation problems connected with the motion of small particles suspended in a turbulent fluid," Ph.D. thesis (Martinus Nijhoff, Delft, The Hague, 1947).
[18]S. Corrsin and J. Lumley, "On the equation of motion for a particle in turbulent fluid," Appl. Sci. Res., Sect. A **6**, 114 (1956).
[19]M. R. Maxey and J. J. Riley, "Equation of motion for a small rigid sphere in a nonuniform flow," Phys. Fluids **26**, 883–889 (1983).
[20]M. R. Maxey, "The motion of small spherical particles in a cellular flow field," Phys. Fluids **30**, 1915–1928 (1987).
[21]R. W. Mei, R. J. Adrian, and T. J. Hanratty, "Particle dispersion in isotropic turbulence under Stokes drag and Basset force with gravitational setting," J. Fluid Mech. **225**, 481–495 (1991).
[22]R. W. Mei, "Flow due to an oscillating sphere and an expression for unsteady drag on the sphere at finite Reynolds number," J. Fluid Mech. **270**, 133–174 (1994).
[23]J. Feng, H. H. Hu, and D. D. Joseph, "Direct simulation of initial-value problems for the motion of solid bodies in a Newtonian fluid. 1. Sedimentation," J. Fluid Mech. **261**, 95–134 (1994).
[24]J. Feng, H. H. Hu, and D. D. Joseph, "Direct simulation of initial-value problems for the motion of solid bodies in a Newtonian fluid. 2. Couette and Poiseuille flows," J. Fluid Mech. **277**, 271–301 (1994).
[25]M. Jenny, J. Dušek, and G. Bouchet, "Instabilities and transition of a sphere falling or ascending freely in a Newtonian fluid," J. Fluid Mech. **508**, 201–239 (2004).
[26]Z. S. Yu, N. Phan-Thine, and R. I. Tanner, "Dynamic simulation of sphere motion in a vertical tube," J. Fluid Mech. **518**, 61–93 (2004).
[27]M. Horowitz and C. H. K. Williamson, "The effect of Reynolds number on the dynamics and wakes of freely rising and falling spheres," J. Fluid Mech. **651**, 251–294 (2010).
[28]T. Deloze, Y. Hoarau, and J. Dušek, "Transition scenario of a sphere freely falling in a vertical tube," J. Fluid Mech. **711**, 40–60 (2012).
[29]D. R. Oliver, "Influence of particle rotation on radial migration in Poiseuille flow of suspensions," Nature **194**, 1269–1271 (1962).

[30]P. G. Saffman, "On the motion of small spheroidal viscous liquid particles in a viscous liquid," J. Fluid Mech. **1**, 540–553 (1956).
[31]P. G. Saffman, "The lift on a small sphere in a slow shear flow," J. Fluid Mech. **22**, 385–400 (1965).
[32]D. W. Moore and P. G. Saffman, "The rise of a body through a rotating fluid in a container of finite length," J. Fluid Mech. **31**, 635–642 (1968).
[33]G. Segre and A. Silberberg, "Behaviour of macroscopic rigid spheres in Poiseuille flow Part 2. Experimental results and interpretation," J. Fluid Mech. **14**, 136–157 (1962).
[34]J.-P. Matas, J. F. Morris, and E. Guazzelli, "Inertial migration of rigid spherical particles in Poiseuille flow," J. Fluid Mech. **515**, 171–195 (2004).
[35]T.-W. Pan, A. Li, and R. Glowinski, "Numerical study of equilibrium radial positions of neutrally buoyant balls in circular Poiseuille flows," Phys. Fluids **33**, 033301 (2021).
[36]Y. Morita, T. Itano, and M. Sugihara-Seki, "Equilibrium radial positions of neutrally buoyant spherical particles over the circular cross-section in Poiseuille flow," J. Fluid Mech. **813**, 750–767 (2017).
[37]S. Nakayama, H. Yamashita, T. Yabu, T. Itano, and M. Sugihara-Seki, "Three regimes of inertial focusing for spherical particles suspended in circular tube flows," J. Fluid Mech. **871**, 952 (2019).
[38]O. Aouane, M. Sega, B. Bäuerlein, K. Avila, and J. Harting, "Inertial focusing of a dilute suspension in pipe flow," Phys. Fluids **34**, 113312 (2022).
[39]A. J. Fox, J. W. Schneider, and A. S. Khair, "Dynamics of a sphere in inertial shear flow between parallel walls," J. Fluid Mech. **915**, A119 (2021).
[40]P. Shi and R. Rzehak, "Lift forces on solid spherical particles in wall-bounded flows," Chem. Eng. Sci. **211**, 115264 (2020).
[41]N. I. K. Ekanayake, J. D. Berry, A. D. Stickland, D. E. Dunstan, I. L. Muir, S. K. Dower, and D. J. E. Harvie, "Lift and drag forces acting on a particle moving with zero slip in a linear shear flow near a wall," J. Fluid Mech. **904**, A6 (2020).
[42]R. C. Jeffrey and J. R. Pearson, "Particle motion in laminar vertical tube flow," J. Fluid Mech. **22**, 721–735 (1965).
[43]A. Karnis, H. L. Goldsmith, and S. G. Mason, "The flow of suspensions through tubes V. Inertial effects," Can. J. Chem. Eng. **44**, 181–193 (1966).
[44]J. A. Schonberg and E. J. Hinch, "Inertial migration of a sphere in Poiseuille flow," J. Fluid Mech. **203**, 517–524 (1989).
[45]R. Mei, "An approximate expression for the shear lift force on a spherical particle at finite Reynolds number," Int. J. Multiphase Flow **18**, 145–147 (1992).
[46]E. S. Asmolov, "The inertial lift on a spherical particle in a plane Poiseuille flow at large channel Reynolds number," J. Fluid Mech. **381**, 63–87 (1999).
[47]E. S. Asmolov, T. V. Nizkaya, J. Harting, and O. I. Vinogradova, "Instability of particle inertial migration in shear flow," Phys. Fluids **33**, 092008 (2021).
[48]L. G. Leal, "Particle motion in a viscous fluid," Annu. Rev. Fluid Mech. **12**, 435–476 (1980).
[49]P. Vasseur and R. G. Cox, "The lateral migration of spherical particles sedimenting in a stagnant bounded fluid," J. Fluid Mech. **80**, 561–591 (1977).
[50]X. M. Shao, Z. S. Yu, and B. Sun, "Inertial migration of spherical particles in circular Poiseuille flow at moderately high Reynolds numbers," Phys. Fluids **20**, 103307 (2008).
[51]J.-P. Matas, J. F. Morris, and E. Guazzelli, "Transition to turbulence in particulate pipe flow," Phys. Rev. Lett. **90**, 014501 (2003).
[52]J.-P. Matas, J. F. Morris, and E. Guazzelli, "Lateral forces on a sphere," Oil Gas Sci. Technol. **59**, 59 (2004).
[53]B. Bai, H. Jin, P. Liu, W. Wang, and J. Zhang, "Experimental study on the equilibrium position of a falling sphere in a circular tube flow," Int. J. Multiphase Flow **153**, 104112 (2022).
[54]L. Liu, J. Yang, H. Lu, X. Tian, and W. Lu, "Numerical simulations on the motion of a heavy sphere in upward Poiseuille flow," Ocean Eng. **172**, 245 (2019).
[55]C.-C. Liao, W.-W. Hsiao, T.-Y. Lin, and C.-A. Lin, "Simulations of two sedimenting-interacting spheres with different sizes and initial configurations using immersed boundary method," Comput. Mech. **55**(6), 1191–1200 (2015).
[56]D. Nie and J. Lin, "Simulation of sedimentation of two spheres with different densities in a square tube," J. Fluid Mech. **896**, A12 (2020).
[57]W. Ren, X. Zhang, Y. Zhang, P. Li, and X. Lu, "Investigation of particle size impact on dense particulate flows in a vertical pipe," Phys. Fluids **35**(7), 073302 (2023).
[58]C. Wan, S. Xiao, D. Zhou, H. Zhu, Y. Bao, K. Kakanda, and Z. Han, "Numerical simulation on transport behavior of gradated coarse particles in deep-sea vertical pipe transportation," Phys. Fluids **35**(4), 043328 (2023).
[59]Y. Dai, Y. Zhang, and X. Li, "Numerical and experimental investigations on pipeline internal solid-liquid mixed fluid for deep ocean mining," Ocean Eng. **220**, 108411 (2021).
[60]M. Zhou, S. Wang, S. Kuang, K. Luo, J. Fan, and A. Yu, "CFD-DEM modelling of hydraulic conveying of solid particles in a vertical pipe," Powder Technol. **354**, 893–905 (2019).
[61]Q. Chen, T. Xiong, X. Zhang, and P. Jiang, "Study of the hydraulic transport of non-spherical particles in a pipeline based on the CFD-DEM," Eng. Appl. Comput. Fluid Mech. **14**, 53–69 (2020).
[62]Y. Zhang, X.-B. Lu, and X.-H. Zhang, "Numerical simulation on transportation behavior of dense coarse particles in vertical pipe with an optimized Eulerian–Lagrangian method," Phys. Fluids **34**(3), 033305 (2022).
[63]A. Renzo and F. Maio, "Comparison of contact-force models for the simulation of collisions in DEM-based granular flow codes," Chem. Eng. Sci. **59**(3), 525–541 (2004).
[64]R. Clift, J. R. Grace, and M. E. Weber, *Bubbles, Drops, and Particles* (Academic Press, New York, 1978), pp. 222–229.
[65]E. E. Michaelides and A. Roig, "A reinterpretation of the Odar and Hamilton data on the unsteady equation of motion of particles," AIChE J. **57**(11), 2997–3002 (2011).
[66]P. Kosinski and A. C. Hoffmann, "Extension of the hard-sphere particle-wall collision model to account for particle deposition," Phys. Rev. E **79**(6), 061302 (2009).
[67]P. Gondret, M. Lance, and L. Petit, "Bouncing motion of spherical particles in fluids," Phys. Fluids **14**, 643 (2002).
[68]Z. M. Ji, Y. J. Tang, F. Q. Wu, J. Liu, T. L. Chen, and Z. J. Chen, "Laboratory investigation of the effect of rockfall shape and size on coefficient of restitution," Rock Soil Mech. **42**, 665–672 (2021).